Identification of the electron donor to flavodiiron proteins in Synechocystis sp. PCC 6803 by in vivo spectroscopy

Pierre Sétif, Ginga Shimakawa, Anja Krieger-Liszkay, Chikahiro Miyake

Identification of the electron donor to flavodiiron proteins in Synechocystis sp. PCC 6803 by in vivo spectroscopy

Pierre SÉTIF[1], Ginga SHIMAKAWA[1], Anja KRIEGER-LISZKAY[1] and Chikahiro MIYAKE[2]

[1] Institute for Integrative Biology of the Cell (I2BC), CEA, CNRS, Université Paris-Sud, Université Paris-Saclay, 91198 Gif-sur-Yvette Cedex, France

[2] Department of Biological and Environmental Sciences, Faculty of Agriculture, Kobe University, 1-1 Rokkodai, Nada, Kobe 657-8501, Japan

Correspondence:
pierre.setif@cea.fr Tel.: + 33 169089867

Abstract

Flavodiiron proteins (FDPs) of photosynthetic organisms play a photoprotective role by reducing oxygen to water and thus avoiding the accumulation of excess electrons on the photosystem I (PSI) acceptor side under stress conditions. In *Synechocystis* sp. PCC 6803 grown under high CO_2, both FDPs Flv1 and Flv3 are indispensable for oxygen reduction. We performed a detailed *in vivo* kinetic study of wild-type (WT) and Δ*flv1/3* strains of *Synechocystis* using light-induced NADPH fluorescence and near-infrared absorption of iron-sulfur clusters from ferredoxin and the PSI acceptors (F_AF_B), collectively named FeS. These measurements were performed under conditions where the Calvin-Benson cycle is inactive or poorly activated. Under such conditions, the NADPH decay following a short illumination decays in parallel in both strains and exhibits a time lag which is correlated to the presence of reduced FeS. On the contrary, reduced FeS decays much faster in WT than in Δ*flv1/3* (13 *vs* 2 s^{-1}). These data unambiguously show that reduced ferredoxin, or possibly reduced F_AF_B, is the direct electron donor to the Flv1/Flv3 heterodimer. Evidences for large reduction of (F_AF_B) and recombination reactions within PSI were also provided by near-infrared absorption. Mutants lacking either the NDH1-L complex, the homolog of complex I of respiration, or the Pgr5 protein show no difference with WT in the oxidation of reduced FeS following a short illumination. These observations question the participation of a significant cyclic electron flow in cyanobacteria during the first seconds of the induction phase of photosynthesis.

Introduction

Photosynthetic organisms have developped multiple protective mechanisms to cope with environmental conditions leading to overreduction of the electron-transfer chain, which can be highly deleterious and lead to photoinhibition processes in the presence of oxygen. In cyanobacteria and other oxygenic phototrophs including green algae, mosses and gymnosperms, but not angiosperms, flavodiiron proteins (FDPs) play such a role by oxidizing cytoplasmic/stromal reductants resulting from photosystem I (PSI) activity and reducing oxygen directly to water [1,2]. FDPs are also found in anaerobes where they can reduce either nitric oxide or transiently-present O_2, protecting them against oxidative stress [3]. FDPs can be grouped in several classes containing different domains [4]. The two N-terminal domains constitute the enzymatic core of all FDPs: a β-lactamase domain containing 2 irons (diiron site) and a FMN-containing flavodoxin domain. Crystallographic structures of bacterial FDPs (see *e.g.* [5,6] revealed that the diiron cluster, the site at which O_2 is reduced, and the FMN moeity of these 2 domains are too far apart (≈ 40 Å) for electron exchange between them and that the minimal functional unit is a head-to-tail dimer which involves one diiron site of a monomer and a close-by FMN from the other one.

Photosynthetic FDPs are composed of 3 domains: from the N to C-terminus, the β-lactamase domain, the flavodoxin domain and a flavin-reductase domain. This last domain binds FMN or FAD, is capable of NAD(P)H

oxidation and has been found to link NADH oxidation to O_2 reduction in a purified FDP protein [7]. The cyanobacterium *Synechocystis sp.* PCC 6803 (thereafter named *Syn*. 6803) contains 4 different FDP genes *flv1* to *flv4* [8]. Whereas the Flv3 and Flv4 proteins have the canonical putative diiron ligands (including acidic residues) similar to those found in FDPs from anaerobes, Flv1 and Flv2 have not and it is still unclear if they can bind iron and reduce O_2 at their presumed enzymatic site [9]. In photosynthetic organisms, FDPs can be grouped in two different phylogenetic clusters, with *Syn*. 6803 Flv1/2 and Flv3/4 belonging to either group. From our present knowledge, FDPs often appear to function in pairs composed of one member of each cluster (Flv1/3 and Flv2/4 in the case *Syn*. 6803) [10,11]. This supports the idea that a FDP functional unit of a photosynthetic organism consists in most cases of a heterodimer composed of monomers of either cluster [11]. In *Syn*. 6803, both Flv2 and Flv4 contribute to O_2 photoreduction when cells are grown under low CO_2 [12,13] whereas it was first found that both Flv1 and Flv3 are indispensable for O_2 photoreduction under high CO_2 conditions [8], as confirmed later on [14]. Whereas the *Δflv1/3* mutant grows similarly to WT under continuous light and both high and low CO_2, Flv1 and Flv3 proteins are both necessary for growth under highly-fluctuating light [14,15]. This is attributed to protection by Flv1/3 as a safety valve for excess electrons on the PSI acceptor side, which impedes the formation of ROS species. A similar protective function of FDPs has been documented in all photosynthetic organisms where they were either deleted [16-20] or newly introduced in the case of angiosperms [21-24].

In vitro activity studies of photosynthetic FDPs were performed with *Syn*. 6803 proteins in their homo-oligomeric forms, with homodimers being presumably the minimal functional units. In these studies, NAD(P)H-dependent O_2 reduction was measured, with activities ranging from very small [7] and small [12] to high [25]. These *in vitro* activities are consistent with the presence of a 3rd C-terminal domain. In addition, homo-oligomers of Flv1 and Flv3 were shown to be involved in acclimation of *Syn*. 6803 cells to fluctuating light, in relation with an unknown activity different from O_2 reduction [14].

During photosynthesis, different modes of electron flow can occur: besides the major linear one from water to $NADP^+$, alternative electron flows are thought to be involved in regulation, photoprotection and adjustment of the ATP to NADPH ratio. Photosynthetic FDPs are thus the terminal components in a Mehler-like or water to water electron flow. Cyclic electron flow is also considered to be an important pathway, which is thought to involve mostly the NDH-1L complex in cyanobacteria, although another pathway using the protein Pgr5 is still a subject of study [26]. NDH-1L, an analog of complex I of respiration, reduces the plastoquinone pool of photosynthetic membranes by using Fd_{red} as electron donor [27,28]. This Fd_{red}-oxidation activity of NDH-1L may involve a NDH-1L/PSI supercomplex which has been detected in *Syn*. 6803 [29].

PSI is a light-driven plastocyanin (Pcy)-ferredoxin (Fd) oxidoreductase [30-32]. Pcy and Fd are soluble electron carriers located at either side of the photosynthetic membrane. PSI charge separation leads rapidly to the state $P700^+$ $(F_A\ F_B)_{1red}$ (1red for singly reduced), where P700 is a chlorophyll (Chl.) dimer and (F_A F_B) are two [4Fe-4S] clusters in fast redox equilibrium. $P700^+$ is reduced by Pcy, thus giving Pcy_{ox} (oxidized Pcy) on the lumenal side of the membrane whereas Fd, containing a [2Fe-2S] cluster, is reduced by $(F_A\ F_B)_{1red}$ at the other side. Moreover F_B, the most exposed PSI cluster, is the electron-transfer partner of Fd. Fd_{red} (reduced Fd) has many redox partners, the most important being ferredoxin-$NADP^+$-oxidoreductase (FNR) which reduces $NADP^+$ to NADPH.

Beside the comparison of growth rates and light sensitivities under different conditions, the physiological and functional characterization of FDP deletion mutants was performed, mostly in *Syn*. 6803, by a large variety of methods including gas exchange measurements, gene and protein expression, near-infrared (NIR) P700 absorption and Chl. fluorescence. None of these techniques addresses directly the consumption by FDPs of stromal/cytoplasmic reductants (Fd_{red}, NADPH) generated by PSI under light. At present, it is not yet established that NADPH is the electron donor to Flv *in vivo*, although this is suggested by the NAD(P)H-oxidizing activity of purified FDPs from *Syn*. 6803. To investigate this point, we combined in the present work measurements of NADPH fluorescence and Fd absorption in WT and Δ*flv1/3* strains from *Syn*. 6803. Fd measurements were performed with a recently available NIR-transmission spectrophotometer, which allows the measurement of redox changes of Fd together with that of P700 and Pcy [33-35].

Materials and methods

Biological materials

WT and mutant strains are from *Syn*. 6803. The Δ*flv1/3* mutant was made as previously described [20]. The Δn*dhD1/D2* mutant was a gift of Prof. Sonoike (Waseda University, Japan) and was constructed by Ohkawa et al. [36] . The mutant deficient in the gene coding for Pgr5 (*ssr2016*) was made as follows. Part of the gene region was replaced with the kanamycin resistance gene (*Kan*^{r}) amplified from the pUC4-KIXX vector [12]. The genomic regions containing *pgr5* were separately amplified by PCR, using gene-specific UP and DN primer sets (UP f: CCGTCCCGGACAAATGGTGGATA; UP r: AAACCGCCCAGTCTACAGTGGAGGGCAATCGCCTTAC; DN f: GTTGGGCTTCGGAATCATCGATGCCAAACAGCGCCA; DN r: GGAGAATGGTTTCCACCGAAGG). The three fragments, including UP, *Kan*^{r}, and DN were linked by successive PCR to obtain disruption cassettes, and *Syn*. 6803 was transformed using the standard procedure described by Williams [37]. The mutant (Δ*pgr5*) was selected on BG-11 agar plates that contained kanamycin (20 µg mL^{-1}). Complete segregation was confirmed using PCR (Supplemental Fig. SI1).

WT and mutant strains of *Syn*. 6803 strains were grown at 25°C in BG-11, buffered at pH 7.5 by 20 mM TES-KOH, on a rotary shaker with a light intensity of 150 µmoles photons m^{-2}s^{-1} in 2% CO_2. For measurements, cells were harvested at a concentration of 6-8 µg Chl./mL, pelleted by centrifugation at 4,000 *g* for 5 minutes and resuspended in fresh BG-11 at a concentration of *c*. 4 and 13 µg Chl./mL for most measurements of NADPH fluorescence and NIR absorption, respectively. Chl. content was measured as previously described [38].

Spectroscopic measurements

Light-induced NADPH fluorescence measurements were performed with a Dual-PAM spectrophotometer (Walz, Effeltrich, Germany) as previously described [39]. The measuring frequency (MF) was kept at a constant value (100 Hz) and was not increased during illumination, contrary to what was advised [40] and previously done [39], as such an increase was found to result in a small artefactual vertical shift of the signal level, which impedes to measure precisely the duration of lags preceding fluorescence decay at cessation of illumination.

Light-induced redox changes of P700, Pcy and Fd were measured with a DUAL-KLAS-NIR spectrophotometer (Walz, Effeltrich, Germany) as previously described [38]. All measurements were performed at 25°C in the "Slow kinetics mode" at a minimal sampling interval of 1 ms.

For NADPH fluorescence measurements, it is needed to centrifuge cells before resuspending them in a fresh medium (BG-11), because of a strong background fluorescence [40]. As our present work deeply relies on combined measurements of NADPH fluorescence and DUAL-KLAS-NIR absorption, we used for all samples the same centrifugation/resuspension treatment, also followed in most cases by dark adaptation for at least 8 mins, for both types of measurements.

DUAL-KLAS-NIR preliminary and control measurements

Deconvolution of the DUAL-KLAS-NIR transmission signals requires the knowledge of the spectral shapes (which will hereafter be named DMPs, *i.e*. differential model plots) of the 3 species to be deconvoluted, *i.e*. P700, Pcy and Fd. It has been shown in a recent *in vitro* study that the terminal acceptors (F_A F_B) of PSI give a DMP similar to that of Fd [41]. Moreover it has also been shown that, if Fd and (F_A F_B) are both reduced by illumination, their signals could be measured together in an additive way. As our results will show that (F_A F_B) are indeed reduced during our measurements, the so-called Fd contribution will be renamed "FeS" in the present work, in order to underline that it may arise from both the [2Fe-2S] cluster of Fd and the [4Fe-4S] clusters of PSI.

Procedures involving different light/dark (pre)treatments have been proposed to measure *in vivo* the individual DMPs of P700, Pcy and Fd/FeS [33]. These recipes rely on the possibility to get a signal change which is selective for one species while the two others give negligible contributions. For Fd/FeS, the published procedure (Fig. 6 in [33] was used with only a change in the illumination time (300-400 ms). Measuring the P700 and Pcy DMPs (Fig. 7 and 8 in [33], respectively) requires an adaptation of the procedures, due to the fact that the PSI/PSII ratio is much larger in *Syn*. 6803 (≥ 3) than in plants (≈ 1). To compensate for the small relative amount of PSII, it was necessary for both types of measurements to replace the single turnover flash

by a series of flashes or a longer high-intensity illumination in order to increase the amount of PSII-originating electrons driving $P700^+$ and Pcy_{ox} reduction. For both types of measurements (P700 and Pcy), either 3 to 6 single turnover (ST) flashes separated by 1 ms time intervals or a single MT flash of *c*. 5 ms was found to allow pure species to be measured. The *Syn*. 6803 DMPs measured *in vivo* and used in the present study are given in Fig. SI2. All DMPs were measured with the same WT strain (+ the Δ*flv1/3* mutant in Kobe) using 2 different DUAL-KLAS-NIR spectrophotometers located either in Kobe University or in Saclay laboratory. For each chemical species, its DMPs differ somewhat when measured in one laboratory or another. This should be related to the fact that the LEDs emission spectra slightly differ from one spectrophotometer to another (Dr. C. Klughammer, personal communication).

A procedure allowing determination of the 100% amplitudes of P700, Pcy and FeS signals has also been described [34]. This procedure was adapted to measure these amplitudes in the different strains by reference to an amplitude of 1 for P700.

The relative absorption coefficients of P700, Pcy, Fd and (F_A F_B) at 902.5 nm were previously determined *in vitro* for tobacco and *T. elong.* [41]. These values can also be calculated for *Syn*. 6803 from data in this last paper and are given in Table 1. In the description of some of the results, it will be assumed that these values can be extrapolated to *in vivo* measurements, as supported by the fact that quasi-ideal conditions of light transmission appear to be met with *Syn*. 6803 cells.

Methyl viologen (MV) at 300 µM is known to oxidize Fd_{red} and $(F_A\ F_B)_{red}$ *in vitro* in the millisecond timerange and it should inhibit the stationary formation of both reduced species *in vivo* [42]. Fig. SI3 shows the effect of MV addition on *in vivo* signals of P700, Pcy and FeS, with signals shown in percent of their maximal amplitude. Whereas the transient reduction of $P700^+$ is inhibited by MV addition and the Pcy signal is little modified, the FeS signal has considerably decreased 7-9 minutes after MV addition and has completely disappeared 10 minutes after. This gives evidence that FeS are indeed correctly identified and measured through deconvolution of NIR signals.

Results

NADPH fluorescence of WT and Δ*flv1/3*

Since NADPH has been proposed to be the electron donor to FDPs, first we measured the light-induced kinetics of NADPH fluorescence in WT and Δ*flv1/3*. Such fluorescence kinetics were previously studied in detail in WT [39]. Whereas NADH can also contribute to the signals as its fluorescence is identical to that of NADPH, the kinetic properties of the light-induced signals, such as the fast rise at light onset and the light activation of decay, indicate that the most part of the light-dependent fluorescence signals can be attributed to NADPH. In the following, we will assume that this is indeed the case. The fluorescence kinetics were compared under different conditions of continuous illumination. Identical kinetics are observed for the fluorescence rise at the onset of illumination (Fig. 1, Fig. SI4) and the fluorescence decay after a prolonged illumination, when the Calvin-Benson cycle (CBc) is activated (Fig. 1/D). The similarity in rising kinetics suggests that the FNR content of both strains is similar. After prolonged illumination, the similarity in decay kinetics shows that the presence of Flv1/3 has no observable effect on NADPH decay, when the activated CBc drives a high NADPH consumption.

NADPH kinetics were also studied with a short illumination period of 400 ms (Fig. 1/ABC). This duration was chosen as it is long enough to elicit a full fluorescence rise whereas it only weakly activates the CBc [39]. Moreover signal averaging was performed at a time interval of 1 min., which should allow significant CBc deactivation between 2 consecutive measurements (note however that the signal undershoot observed at t > 4-5 s in Fig. 1/A is diagnostic of the activation of a NADPH consuming enzyme, corresponding presumably to partial CBc activation). Under these conditions, the fluorescence decay is, as expected, slower than after CBc activation. Thus the time needed for 50% signal decay is 2.2 and 2.65 s for WT and Δ*flv1/3*, respectively, whereas, after 120 s illumination, this time drops to 0.38 and 0.36 s for WT and Δ*flv1/3*, respectively.

For evaluating the Flv1/3 involvement in NADPH oxidation, it is required to compare post-illumination decay kinetics without any type of signal normalization. This condition is almost met in Fig. 1 as the Δ*flv1/3* signal

was multiplied by a small factor of 1.04 in order to normalize the light-induced signal allowing us to compare more easily the rising and decay kinetics. This indicates that the NADP photoreducible pools are quite similar in WT and Δ*flv1/3*. We repeatedly compared the NADP-reducible pool sizes in WT and Δ*flv1/3* and found values comprised between 1.03 and 1.15 for the Δ*flv1/3* to WT pool ratio. The similarity in NADP pool sizes is also shown in Fig. SI5, in which NADPH fluorescence is measured at different chlorophyll concentrations.

The longer 50% signal decay time in Δ*flv1/3* after 400 ms illumination seems at first sight to be in accordance with NADPH oxidation by Flv1/3. However this is misleading as it can be seen that fluorescence decays almost in parallel in both strains (Fig. 1/A) and the most conspicuous difference in kinetics is the presence of a lag preceding the decay in Δ*flv1/3* (Fig. 1/B). This decay is *c*. 700 ms long whereas it was clearly visible in WT only after extensive averaging, with a value of 140 ms (Fig. 1/C). It can also be noted that the lag decreases after CBc activation as it was not any longer observed in both strains after 120 s illumination (Fig. 1/D).

The origin of these lags is easily interpreted if one assumes that stromal reductants besides NADPH, *i.e*. Fd_{red} and reduced PSI acceptors (collectively named FeS_{red} in the following), are accumulated in the light and that, after light cessation, these reductants are consumed via FNR catalysis to maintain the NADP pool at its maximum state of reduction. The lag would then correspond to the time it takes for these reductants to be reoxidized. This hypothesis will be tested below by measuring the kinetics of FeS_{red} reoxidation after illumination.

DUAL-KLAS-NIR kinetics of P700, Pcy and FeS in WT and ΔFlv1/3

Kinetics of P700, Pcy and FeS redox changes were first measured in a procedure allowing us to obtain the maximum amplitudes of the 3 species (P700, Pcy and FeS) [34] (Fig. 2). When WT and Δ*flv1/3* kinetics were compared in detail, the following was observed:

1) Following dark adaptation, the P700 kinetics at the onset of actinic light are initially similar in both strains, with a fast rise followed by a fast decay during the first 300-400 ms (Fig. 3). Such observations have already been reported and interpreted as follows [15,43,44]: the initial rise and decay are attributed to PSI charge separation and stabilization followed by reduction by incoming electrons due to PSII activity. After this initial increase/decay pattern, the P700 kinetics strongly differ in WT and ΔFlv1/3, as P700 remains reduced in Δ*flv1/3* whereas $P700^+$ increases to a large level in WT. This large WT level involves a donor-side limitation that has been shown to protect PSI from photooxidative damage [20,45]. This protection involves electron transfer to O_2 catalyzed by Flv1/3. In Δ*flv1/3,* where this flow is absent, the high reduction level of the stromal electron acceptors limits P700 photooxidation, an effect which may involve charge recombination reactions (PSI acceptor-side limitation) or cyclic electron flow [43].

2) The Pcy kinetics follow the P700 kinetics with little Pcy_{ox} accumulated in Δ*flv1/3* after 400 ms.

3) The FeS reduction kinetics are quite similar in WT and Δ*flv1/3* at the onset of actinic light but deviate after 500 ms. Whereas a high level of FeS_{red} remains during illumination in Δ*flv1/3* (signal between 3 and 6 s in Fig. 2/B), FeS_{red} decays in WT, an effect which can be attributed to the fact that P700 becomes almost entirely oxidized during this period. By applying a MT pulse of high intensity at 350 ms, the maximal signal of Fd reduction was claimed to be measurable [34], but this maximal signal will be discussed in detail further below.

The maximal signals due to P700 and Pcy oxidations (Table 2) are obtained by subsequent application of a long MT pulse which is given at the end of a far-red illumination period (10 to 20 s in Fig. 2; [34]). From the chlorophyll content of the samples and the *in vitro* determination of the $P700^+$ coefficient at 902.5 nm with isolated PSI from *Syn*. 6803 [41], theoretical $P700^+$ signals can also be calculated together with amplification factors.

An amplification factor of of 1 would be consistent with ideal optical properties with an optical pathlength corresponding to the cuvette width, *i.e*. with no contribution from light refraction and reflexion within the cells. The fact that these factors are just above 1 for both *Syn*. 6803 strains is in accordance with recent measurements [38] and indicates that the present measurements are made under quasi-ideal conditions of light transmission. In turn, this provides support to the idea that the relative coefficients measured *in vitro* (Table 1) can be extrapolated to *in vivo* conditions in order to estimate the stoichiometries of the different

electron-transfer components. This property was used to calculate Pcy/PSI ratios of 2.2-2.3 in both strains (Table 2).

Kinetics of FeS_{red} reoxidation after a short illumination in WT and Δ*flv1/3*

DUAL-KLAS-NIR kinetics were further studied with the same samples as above using extensive averaging of signals induced by actinic red light of high intensity (8100 µmoles photons $m^{-2}s^{-1}$) and 350 ms duration (Fig. 3, Fig. 4/traces b and d). This duration is optimal for 3 reasons, *i.e*. just completed $NADP^+$ photoreduction (Fig. 1/B), limited activation of the CBc and minimal extent of P700/Pcy photooxidation. Moreover, the difference in $P700^+$ and Pcy_{ox} levels between WT and Δ*flv1/3* are relatively small at the end of illumination, so that the subsequent dark FeS_{red} decays can be compared with minimal interferences from recombination reactions and imperfect 3-species deconvolutions. A significant level (35%) of P700 oxidation is though observed in WT, contrary to Δ*flv1/3*. However , at the end of illumination, the P700 signal decays much faster than the FeS signal. This implies that no or very little recombination is involved in the WT FeS_{red} decay. From Figs. 3 and 4, it can be seen that FeS_{red} decays much more slowly in Δ*flv1/3* than in WT whereas light-induced FeS reductions are quite similar. Similar FeS_{red} decay kinetics were also measured after illumination with a light intensity similar to that used for $NADP^+$ photoreduction (traces a and c in Fig. 4). Monoexponential fits of Fd_{red} give values 13.1-13.3 s^{-1} and 2.3-2.4 s^{-1} in WT and Δ*flv1/3*, respectively. This difference in FeS decay kinetics between WT and Δ*flv1/3* fits nicely with the different lags that were observed for NADPH decay in the 2 strains.

These observations confirm our hypothesis that the lags observed in NADPH decays correspond to consumption of FeS_{red} by FNR, which maintains the NADP pool at its fully reduced level as long as some FeS_{red} is available. Moreover, and more importantly, the difference in FeS_{red} oxidation kinetics between WT and Δ*flv1/3* in combination with the slower and identical NADPH decays (disregarding the lags) shows that Flv1/3 accept electrons upstream from NADPH, at the FeS_{red} level.

Evidence for recombination between $P700^+$ and F_{Xred}. Contribution of Fd to the NIR FeS signal

Schreiber and Klughammer [34] published a procedure for measuring the maximal NIR signal of Fd reduction by applying an intense MT pulse superimposed on a high intensity actinic light under conditions where the CBc is not activated, so that Fd_{red} reoxidation is relatively slow (Fig. 2). This determination implicitly relies on the idea that Fd_{red} can be fully accumulated without NIR contribution due to reduction of the [4Fe-4S] terminal PSI acceptors. However *in vitro* measurements recently showed that (F_A F_B) reduction can contribute to NIR signals [41]. It is also expected that reduction of F_X, the [4Fe-4S] preceding (F_A F_B) in PSI, should give as well a NIR contribution. Moreover, if PSI [4Fe-4S] acceptors are reduced, they could be involved in subms to 100 ms recombination reactions, so that their stationary reduction state may highly depend on the light intensity and be possibly incomplete. To examine this matter, we extensively averaged signals under the above conditions to check whether we can obtain evidence for recombination reactions. A sample similar to that studied above was submitted to high intensity red light for 1 s to which a 100 ms MT pulse of very high intensity was superimposed between 300 and 400 ms after the onset of actinic light. The measurements were made at a low repetition rate in order to minimize CBc activation. The WT results shown in Fig. 5A, where P700, Pcy and FeS signals are plotted with Y-scales proportional to their relative differential absorption coefficients (Table 1), suggest that recombination occurs between $P700^+$ and F_{Xred} at the end of the MT pulse (t = 0.4 s). This is seen as an unresolved step signal (sampling time is 1 ms), which exhibits a signal ratio FeS/P700 of -0.079. This ratio is 1.8 times larger than the $(F_A\ F_B)_{single\ red.}$/P700 ratio of -0.044 (Table 1), a difference which may be attributed either to imperfect deconvolution or to a NIR differential absorption of F_X larger than that corresponding to single reduction of (F_A F_B). The same measurements were performed with Δ*flv1/3* (Fig. 5B) with results qualitatively similar to those of WT, but with a smaller amplitude of both P700 and FeS signals that can be attributed to fast recombination between $P700^+$ and FeS_{red}. The reason why the signals attributed to recombination are smaller in Δ*flv1/3* than in WT may be that some F_{Xred} is partially accumulated in Δ*flv1/3* before the MT pulse. This interpretation is in accordance with the larger acceptor side limitation in this strain.

Assuming the above conclusion about F_X involvement in NIR absorption, the maximal FeS signal observed in Figs. 3 and 4 should then correspond to both Fd and (F_A F_B) fully reduced. In turn, by using the relative absorption coefficients measured *in vitro* (Table 1), the (F_A F_B) contribution was estimated to 71-74% of this maximal signal in both WT and ΔFlv1/3 whereas the minor Fd signal would correspond to a Fd/PSI ratio of 1.1-1.4, in agreement with [46]. There is quite evidently a large uncertainty in this last estimation and more work is needed to derive the Fd/PSI ratio in cyanobacteria from NIR measurements. However we would like to emphasize here that the FeS signal most probably includes a large, and possibly major, contribution of (F_A F_B) reduction.

FeS accumulates more rapidly when the NADP is highly reduced

Experiments shown in Fig. 6A/B are similar to those of Fig. 4, except for a lower intensity and a longer, but still short, illumination with actinic light. Moreover, the initial FeS kinetics (traces a) were compared to those induced by a second illumination given after a delay just sufficient for FeS_{red} reoxidation (traces b; delay between the end of 1st and beginning of 2nd = 0.4 and 0.9 s for WT and Δ*flv1/3*, respectively). These delays are short enough to allow NADPH to be still almost entirely reduced at the beginning of the 2nd illumination (Fig. 1). For both strains, FeS_{red} reduction is faster during the 2nd illumination since the sigmoidal pattern occurring around 100 ms during the 1st illumination is no longer present. These data can be simply interpreted by assuming that sigmoidicity arises from fast Fd_{red} consumption by FNR which occurs as long as $NADP^+$ is not fully reduced. This interpretation also fits with the kinetics of NADPH fluorescence rise as, during 1st hν measurements, the FeS reduction resumes (or the lag ends) at *c*. 100 ms, a time at which most of NADPH is formed (Fig. 1B). When the delay separating the two illumination periods is long enough for large reoxidation of NADPH, the FeS_{red} kinetics (traces c) are back to those obtained at the 1st illumination. These kinetic changes are also displayed in Fig. 6C by plotting the signal at 100 ms after the beginning of the 2nd illumination as a function of the delay between the illuminations. The presence of a lag in both strains is consistent with a FNR reduction process being dominant as long as the NADP pool is not fully reduced, regardless whether Flv1/3 is present or not. The kinetics following the lag are also rather similar in WT and Δ*flv1/3* (see also Fig. 3). This indicates that Flv1/3 has only a moderate effect on FeS_{red} accumulation under the present conditions of illumination. In turn, this suggests that FeS_{red} accumulation is dictated by reactions faster than reoxidation by Flv1/3, namely donation to $P700^+$ and recombination reactions between $P700^+$ and PSI acceptors and competition between these two processes.

The same measurements were performed with a mutant in which the *pgr5*-like gene was deleted. NIR kinetics in the mutant were virtually identical to those in WT (Fig. 7A) as is also the case for the dependence of the 100-ms signal size upon the delay between the two illuminations (Fig. 7C). This result is consistent with the fact that no significant effect of Pgr5 deletion was previously observed in cyanobacteria [15], although Pgr5 was proposed to be involved in cyclic electron transfer in *Syn*. 6803 [26,47].

The FeS_{red} decay kinetics in the absence of NDH-1L are very similar to those of WT

In a mutant with deleted *ndhD1* and *ndhD2* genes, in which the NDH-1L complex is expected to be absent [48], reoxidation of FeS_{red} after a short illumination was found to be quite similar to those of WT (Fig. 7B). In darkness, the NADP pool was found to be almost entirely reduced in this mutant (Fig. 7D): Illumination of a dark-adapted sample leads only to a small signal increase followed by a similarly small extent of decay (Fig. 7D, trace a). By contrast, a prolonged illumination is followed by a decay of larger amplitude and faster kinetics. Noticeably, the decay kinetics after prolonged illumination are similar to those of WT and Δ*flv1/3* (Fig. 1D), which is attributed to CBc activation in all cases. These data also show that the photoreducible NADP pool is almost entirely reduced in the Δ*ndhD1/D2* mutant in darkness. In accordance with this highly reduced state, the 1st-illumination FeS reduction kinetics (Fig. 7B, trace a) exhibits almost no sigmoidicity and are similar to those of the 2nd-illumination kinetics (Fig. 7B, trace b) as it is also shown from the similarity in the 100-ms signal size for the 2 corresponding illuminations (Fig. 7C). In summary, our observations are in accordance with the fact that the NADP pool remains essentially reduced in Δ*NdhD1/D2* as long as the CBc is not activated and support our interpretation for the 1st-illumination lag observed in the other strains.

Discussion

NIR signals as a tool to measure reduction of Fd and iron-sulfur clusters of PSI

The possibility of recording *in vivo* Fd reduction by real-time NIR spectroscopy has been developped recently [33-35]. This measurement results from deconvolution of NIR signals into contributions of P700, Pcy and Fd. From an *in vitro* NIR study, it has been later determined [41]: 1) that reduction of PSI iron-sulfur clusters is measured together with Fd reduction 2) that cytochrome c_6 oxidation (when present instead of Pcy), and by extrapolation probably also cyt. *f* oxidation, can contribute to NIR signals and 3) that P700 and Pcy oxidations give much larger signals that those attributed to reduction of Fd and PSI clusters. This underlines the difficulty of specifically measuring the kinetics of FeS (collective name for Fd, F_A and F_B) reduction by this method. In the present work, we provide several lines of evidence which show that FeS reduction and reoxidation can indeed be reliably measured in *Syn*. 6803 cells: 1) the FeS signal is no longer observed after incubation with MV (Fig. SI3); 2) the initial FeS reduction kinetics strongly depend on the redox state of the NADP pool at the onset of illumination (Figs. 6 & 7); 3) the FeS_{red} reoxidation kinetics following a short illumination are different in WT and Δ*flv1/3* (Figs. 3-4), contrary to those of $P700^+$ and Pcy_{ox} reduction kinetics which are quite similar (Fig. 3), and these reoxidation kinetics are consistent with the variable NADPH lag observed in both strains (Fig. 1). The global internal consistency of our data provides strong support to the idea that FeS reduction can indeed be measured, even though one cannot exclude that a minor part of the signals attributed to FeS results from imperfect deconvolution or from contribution of other species such as cyt. *f*. In this respect, it should be noted that Pcy is largely expressed in our conditions of cell growth so that we expect little, if any, cyt. c_6 contribution.

Fd_{red} (or F_{Bred}), and not NADPH, is the electron donor to Flv1/3

The presence of both Flv1 and Flv3 proteins is indispensable for oxygen photoreduction in *Syn*. 6803 under high-CO_2 conditions [8] which strongly suggests, but does not prove, that the Flv1/3 heterodimer is responsible for this activity. In the following, we will implicitly assume that this is the case. We compared high-CO_2 grown *Syn*. 6803 WT and Δ*flv1/3* by a combination of 2 different *in vivo* spectroscopic probes, NADPH fluorescence and NIR absorption decrease due to FeS reduction. Most measurements were performed under specific conditions expected to enhance the difference between WT and Δ*flv1/3*, where the PSI acceptor side is highly photoreduced at the end of the illumination period whereas the CBc is weakly activated. This allowed us to conclude that Fd_{red}, or possibly the terminal acceptor F_{Bred} of PSI, and not NADPH, is the redox partner of Flv1/3. The possibility that Fd is an interacting partner of Flv proteins has been previously proposed from Fd-chromatography in *Syn*. 6803 [49], from a 2-hybrid assay study in *Chlamydomonas reinhardtii* [50] and from a recent study showing that, after a short illumination period, Fd_{red} is reoxidized more slowly in the absence of Flv3 [51].

The uncertainty about the exact nature of the Flv1/3 partner (Fd_{red} or F_{Bred}) derives firstly from the fact that the reduction of Fd and of the PSI [4Fe-4S] clusters cannot be spectrally distinguished and are measured in an additive manner and secondly from the observation that Fd, F_A and F_B appear to be all photoreduced during our measurements (Fig. 3 and 4), as deduced by the likely observation of a recombination reaction between $P700^+$ and F_{Xred}, when a very intense pulse light is superimposed to the light period (Fig. 5). If F_{Bred} is the partner of Flv1/3, then Fd_{red} oxidation by Flv1/3 could also proceed indirectly via uphill population of F_{Bred}, so that it should be slower than F_{Bred} oxidation itself, and *a fortiori* slower than (F_{Ared}, F_{Bred}) oxidation. In turn, the decay of FeS_{red} in WT should be multiexponential (Fig. SI6/E), which is not seen in the fits of Fig. 4A. However we estimate that the present signal-to-noise ratio of our measurements of FeS_{red}, together with the uncertainties in the precise deconvolution of the NIR signals, does not allow us to decide for the absence or presence of several exponential components. Thus we cannot definitely conclude from the shape of the FeS_{red} decay whether Fd_{red} or F_{Bred} is the Flv1/3 partner. It is also noticeable that the possibility that F_{Bred} is the partner of Flv1/3 is related to the *in vivo* ratio of Flv1/3 to PSI, as a small ratio seems to be incompatible with an efficient oxidation of F_{Bred} by Flv1/3. To our knowledge, this ratio has yet not been determined.

The fact that NADPH is not the main electron donor to Flv1/3 appears surprising in view of the presence in Flv1 and Flv3 of C-terminal domains which are expected to have a NAD(P)H-oxidizing activity, as supported by *in vitro* measurements of purified proteins [7,12,25]. Moreover, the absence *in vivo* of significant Flv1/3-

dependent NADPH-consuming activity, as deduced from our measurements, seems to contradict some recent results [25]. In this paper, NADPH oxidation turnover numbers 25 and 32 s^{-1} were measured under atmospheric levels of O_2 for Flv1 and Flv3, respectively, and similar activities were measured with NADH. In the case of Flv3, biochemical evidence shows that the Flv3 dimer is the functional unit, and it is also most probably the case for Flv1, as supported by cooperativity measurements for both NAD(P)H and O_2 binding [25].

These high activities of Flv1 and Flv3 dimers contradict previous observations that both Flv1 and Flv3 are indispensable for oxygen photoreduction in *Syn*. 6803 [8]. These observations are in accordance with the strong phenotypes resulting from single deletion of either *flv1* or *flv3* [15] or their homologs in other photosynthetic organisms [18,19,52]. It is noticeable that a straightforward interpretation of single deletion mutants is in general not possible as deletion of one gene of a pair decreases or abolishes expression of the other one [15,18]. Nevertheless, one rather clear case has been reported: in the *flv1* deletion mutant of *Syn*. 6803, where oxygen photoreduction is absent, Flv3 is still expressed at a decreased but significant level [15]. This indicates that the Flv3 dimer is probably not active in oxygen reduction in this organism, as also suggested in [14]. The discrepancy with the latest *in vitro* results [25] requires further investigation.

Roles other than NAD(P)H oxidation may be hypothesized for the Flv1/3 C-terminal domains:

1) NAD(P)H oxidation by the flavins of these domains may indeed occur *in vivo* but at a much slower rate than FeS_{red} oxidation. This reaction may also occur in the other direction (see 3).

2) The C-terminal domains may be involved in Fd binding, only by themselves or concomitantly with the flavodoxin domains. The most simple electron transfer pathway would then be linear : $FeS_{red} \rightarrow Flavin_{C\text{-}terDom} \rightarrow FMN_{flavodoxin} \rightarrow$ diiron.

3) Alternately, the electron transfer pathway may be branched with FeS_{red} reducing the flavodoxin FMN: $FeS_{red} \rightarrow FMN_{flavodoxin} \rightarrow$ diiron, and the flavodoxin FMN being a branching point involved in the reaction: $FMN_{flavodoxin} \rightarrow Flavin_{C\text{-}terDom} \rightarrow NAD(P)^+$. During this reaction, the role of the C-terminal domains would be to store electrons, or even to reduce $NAD(P)^+$. Such reactions could become significant in case of enzyme over-reduction, *i.e*. when the pathway to diiron is slowed down, *e.g.* in low O_2.

The question could be asked whether NADPH decay via FNR-catalysed up-hill population of Fd_{red} followed by electron transfer to Flv1/3 and O_2 reduction could be significant so as to lead to a NADPH consumption faster in WT than in Δ*flv1/3*. This point was checked by numerical simulations and it was found that the NADPH decay should be only weakly accelerated by the presence of Flv1/3 (Fig. SI6/B). However, in all our measurements, such a difference was not observed as the NADPH decay kinetics were either quasi-identical in both strains (Fig. 1 and SI5) or were a little (10% at most) faster in Δ*flv1/3*. This must be attributed to the fact that a non-identified NADPH consuming process is slightly faster in Δ*flv1/3* than in WT (Fig. SI6/D). The presence of a lag in NADPH decay kinetics, which is correlated to the presence of FeS_{red}, has also been reproduced in our simulations (Fig. SI6).

Rates of Fd_{red}/FeS_{red} reoxidation by different partners including FNR, Flv1/3 and NDH-1L.

From the comparison of FeS_{red} decay in WT and ΔFlv1/3 (monoexponential rates of 13.2 and 2.3 s^{-1}, respectively), one can deduce a rate k_{Flv} of 11 s^{-1} for FeS_{red} oxidation by Flv1/3 under the conditions of Fig. 4. As discussed above, the largest part of the light-induced FeS_{red} signal of Fig. 4 probably arises from the terminal PSI acceptors F_A and F_B (Table 2). Therefore k_{Flv} corresponds either to $(F_A\ F_B)_{red}$ oxidation or to Fd_{red} oxidation by Flv1/3 which would limit the rate of $(F_A\ F_B)_{red}$ oxidation:

1) In the former case, Fd reduction by $(F_A\ F_B)_{red}$, a process occurring in the µs-ms time range, would outcompete Flv1/3 reduction by $(F_A\ F_B)_{red}$ by several orders of magnitude. This last process would thus be significant only when Fd is completely reduced;

2) In the latter case, FNR would be the main competitor of Flv1/3 for Fd_{red} oxidation. The *in vivo* kinetics of FNR reduction by Fd_{red} are not known precisely but the kinetics of NADPH formation following a single saturating turnover flash have been measured in *Syn*. 6803 cells. Half of the maximum flash-induced NADPH signal is formed at 8 ms [39], which indicates that the rate k_{FNR} of single electron FNR reduction by Fd_{red} should be significantly faster than 100 s^{-1}. Spectroscopic evidence for a high rate of FNR reduction can also deduced from

the NIR FeS_{red} signal which exhibits a sigmoidal shape when the NADP pool is mostly oxidized (Fig. 6). This underlines that the efficiency of Flv1/3 reduction by Fd_{red} should increase considerably when both FNR and the NADP pool are fully reduced.

We also detected no significant difference in kinetics of FeS_{red} decay between WT and Δ*NdhD1/D2,* in which the NDH-1L complex is absent (Fig. 7B). This result could have been predicted just from the comparison of WT and Δ*flv1/3*, as Flv1/3 is the dominant partner for oxidation of FeS_{red} under both conditions of not active CBc and fully reduced NADP pool. Under these conditions, the oxidation rate of FeS_{red} by all other partners is about 2 s^{-1}. Even if NDH1-L contributes for a significant part to this rate, it would make little difference between WT and Δ*NdhD1/D2* and such a small difference may have escaped detection in our measurements. A more precise comparison of FeS_{red} oxidation using extensive averaging may be required to decide this. It has been previously found that the absence of NDH-1L impedes growth under high-light conditions [53-56]. Moreover, a slow *in vivo* rate of Fd_{red} oxidation by NDH-1L appears to contradict the high rate of NDH-1L reduction by Fd_{red} that was measured *in vitro* [27]. Indeed the second-order rate constant of single NDH-1L reduction was found to be larger than that of FNR reduction. Several non-exclusive possibilities, which could also be related to the different strains involved (*Syn.* 6803 *vs T. elong.*), may explain these apparent discrepancies: 1) firstly, FNR is in large excess over NDH1-L; 2) membrane reorganization favoring recognition efficiency between Fd_{red} and NDH1-L (*e.g*. under high light) increases NDH1-L reduction by Fd_{red}, whereas NDH1-L is distant from PSI under our conditions of measurement; 3) Fd_{red} oxidation by NDH1-L concerns a minor part of Fd having escaped specific identification during our measurements, *e.g*. by involving a small percentage of PSI associated to NDH-1L in a supercomplex [29].

Electron transfer scheme and conclusions

Our work shows that Fd_{red} is the electron donor to Flv1/3 for reducing water to oxygen. However, we cannot exclude that $(F_A\ F_B)_{red}$, the reduced PSI terminal acceptor, can directly reduce Flv1/3. We also obtained evidence that ($F_A\ F_B$) can be highly reduced under continuous illumination and that recombination between $P700^+$ and F_{Xred} is observable *in vivo*. Future work with KLAS-NIR may be useful to clarify the correlation between the redox state of Fd/($F_A\ F_B$) and PSI acceptor side limitation [57], under different conditions including those where the CBc is activated.

Fig. 8 shows an electron transfer scheme involving the acceptor side of PSI. Part A shows the electron transfer rates which were deduced from the present study, corresponding to experimental conditions where FNR and the NADP pool are fully reduced, *i.e.* just after a short illumination with a poorly activated or inactivated CBc (Figures 1, 3-4). From the kinetics of slow FeS_{red} oxidation in Δ*flv1/3*, it can be deduced that Fd_{red} is very slowly oxidized by partners other than FNR (and Flv1/3 in WT): $k_p + k_{inact.} \approx 2\ s^{-1}$, where $k_{inact.}$ is the oxidation rate of NADPH which, *via* FNR, leads to Fd_{red} oxidation (due to residual CBc activity and any processes consuming directly NADPH). In turn, it means that k_p is less than 2 s^{-1}. k_p incorporates all processes of Fd_{red} oxidation by different partners, mostly NDH-1L and soluble partners such as ferredoxin-thioredoxin reductase and redox enzymes for sulfur and nitrogen assimilation, among which nitrite reductase (NiR). One essential issue is to quantify k_p under different types of experimental conditions, as k_p may vary considerably according to these conditions. As an example, we discuss here the specific case of NiR: it may occur that in the conditions of Figures 3-4, both NiR and its substrate nitrite are fully reduced at the end of the illumination period, as it is the case for FNR and its substrate NADP (Fig. 1). If true, this may lead to a very slow Fd_{red} oxidation by NiR (rate k_{pNiR}) which would be limited by ammonium (the product of NiR activity) consumption. Conversely, the k_{pNiR} rate may be much larger in other circumstances, *e.g*. either transiently at the onset of illumination (before full reduction of nitrite) or under a stationary state of illumination, where it is also possible that it is upward regulated. The possibility that k_p is much larger than 2 s^{-1}, *e.g.* when the CBc is activated and the NADP pool partially oxidized, is illustrated in part B of Fig. 8.

With regard to the above discussion, the question should be asked whether NDH-1L reduction by Fd_{red} (rate k_{pNDH1L}) could also be indirectly limited by later steps of the catalytic cycle under the conditions of Figures 3-4, *e.g.* by the availibility of oxidized plastoquinone, its final electron acceptor. If there is no such limitation, it would mean that k_{pNDH1L} is mostly limited by electron transfer from Fd_{red} to NDH-1L. With $k_{pNDH1L} < k_p = 2\ s^{-1}$, this would question the efficiency of NDH-1L involvement in a significant electron flux under light, and more

generally the efficiency of cyclic electron flow in *Syn*. 6803, at least upon onset of actinic light. Future studies aimed at determining the precise FeS_{red} kinetics in different mutants and at various physiological conditions should contribute to answer this question.

Acknowledgements

This work was supported by JST CREST Grant Number JPMJCR15O3 (Japan), by the LabEx Saclay Plant Sciences-SPS (ANR-10-LABX-0040-SPS) and the French Infrastructure for Integrated Structural Biology (FRISBI) ANR-10-INSB-05. It is also partially supported by a grant from the Agence Nationale de la Recherche (RECYFUEL project ANR-16-CE05-0026). G.S. is supported by a JSPS oversea research fellowship (201860126).

Table 1 : Relative differential absorption coefficients in *Syn*. 6803

	Coefficients at 902.5 nm
$P700^+$	1
$Pcy_{ox} – Pcy_{red}$	$0.252^a \pm 0.005^c$
$(F_A F_B)_{1red} - (F_A F_B)_{ox}$	$-0.044^b \pm 0.010$
$Fd_{red} - Fd_{ox}$	$-0.026^b \pm 0.006$

Coefficients at 902.5 nm (840 – 965 nm) were calculated from previous in vitro measurements [41] and are given by reference to a value of 1 for $P700^+$.

[a]Derived from the tobacco coefficient by multiplication by a factor of 1.218 which corresponds to the ratio of the $P700^+$ absorption coefficients of tobacco and *Syn*. 6803 (4.75 and 3.9 $M^{-1}cm^{-1}$, respectively; Table 1 in [41])

[b]Derived from the *T. elong.* coefficient by multiplication by a factor of 1.218 which corresponds to the ratio of the $P700^+$ absorption coefficients of *T. elong.* and *Syn*. 6803 (4.75 and 3.9 $M^{-1}cm^{-1}$, respectively)

[c]Uncertainties values were taken from [41].

Table 2: Maximum signals and relative amounts of the different electron-transfer components in WT and Δ*flv1/3* cells.

	WT		Δ*flv1/3*	
P700 max. value	1.26		1.37	
Calculated signal[a]	1.16		1.19	
Amplification factor[b]	1.09		1.15	
Pcy max. value	0.73		0.77	
n_{Pcy}[c]	2.30 ± 0.05		2.23 ± 0.05	
FeS[d] max. value	-0.15	(100%)	-0.17	(100%)
(F_A F_B) contribution[e]	-0.111 ± 0.025	(74%)	-0.121 ± 0.027	(71%)
Fd contribution[f,h]	-0.039	(26%)	-0.049	(29%)
n_{Fd}[g,h]	1.1		1.4	

Maximum values were determined from Fig. 2 and are given in ($\Delta I/I \times 10^{-3}$) at 902.5 nm. Cells concentrations were 12.5 and 12.8 µg Chl./mL for WT and Δ*flv1/3*, respectively. Relative stoechiometries (n_{Pcy} and n_{Fd}) are given by reference to that of $P700^+$ (= Pcy/PSI and Fd/PSI ratios).

[a]The calculated P700 signal is obtained by assuming a chl./P700 ratio of 108 and an absorption coefficient of 3,900 $M^{-1}cm^{-1}$.

[b]Amplification factor = P700 max. value/Calculated signal.

[c]The number of Pcy per PSI (P700) is calculated using a relative coefficient of 0.252 ± 0.005 (Table 1): *e.g*. for WT, n_{Pcy} = (0.73/1.26)/0.252)

[d]FeS identifies both Fd and the PSI iron-sulfur centers F_A and F_B

[e]The (F_A F_B) contribution is calculated for reduction of both clusters using a relative coefficient (single reduction) of -0.044 ± 0.010 (Table 1) : *e.g*. for WT, (F_A F_B) contribution = -0.044 × 1.26 × 2.

[f]Fd contribution = FeS max. value - (F_A F_B) contribution

[g]Using a relative coefficient of -0.026 (Table 1), which gives, for 1 Fd per PSI, signals of -0.033 and -0.036 for WT and ΔFlv1/3, respectively.

[h]Very large relative uncertainties are not given

References

[1] A. Alboresi, M. Storti, L. Cendron, T. Morosinotto, Role and regulation of class-C flavodiiron proteins in photosynthetic organisms, Biochem. J. 476 (2019) 2487-2498.

[2] Y. Allahverdiyeva, J. Isojarvi, P. Zhang, E. M. Aro, Cyanobacterial Oxygenic Photosynthesis is Protected by Flavodiiron Proteins, Life (Basel, Switzerland) 5 (2015) 716-743.

[3] M. C. Martins, C. V. Romao, F. Folgosa, P. T. Borges, C. Frazao, M. Teixeira, How superoxide reductases and flavodiiron proteins combat oxidative stress in anaerobes, Free Radical Biology and Medicine 140 (2019) 36-60.

[4] F. Folgosa, M. C. Martins, M. Teixeira, Diversity and complexity of flavodiiron NO/O-2 reductases, Fems Microbiology Letters 365 (2018).

[5] C. Frazao, G. Silva, C. M. Gomes, P. Matias, R. Coelho, L. Sieker, S. Macedo, M. Y. Liu, S. Oliveira, M. Teixeira, A. V. Xavier, C. Rodrigues-Pousada, M. A. Carrondo, J. Le Gall, Structure of a dioxygen reduction enzyme from Desulfovibrio gigas, Nature Struct. Biol. 7 (2000) 1041-1045.

[6] C. V. Romao, J. B. Vicente, P. T. Borges, B. L. Victor, P. Lamosa, E. Silva, L. Pereira, T. M. Bandeiras, C. M. Soares, M. A. Carrondo, D. Turner, M. Teixeira, C. Frazao, Structure of Escherichia coli Flavodiiron Nitric Oxide Reductase, J. Mol. Biol. 428 (2016) 4686-4707.

[7] J. B. Vicente, C. M. Gomes, A. Wasserfallen, M. Teixeira, Module fusion in an A-type flavoprotein from the cyanobacterium Synechocystis condenses a multiple-component pathway in a single polypeptide chain, Biochem. Biophys. Res. Comm. 294 (2002) 82-87.

[8] Y. Helman, D. Tchernov, L. Reinhold, M. Shibata, T. Ogawa, R. Schwarz, I. Ohad, A. Kaplan, Genes encoding A-type flavoproteins are essential for photoreduction of O_2 in cyanobacteria, Curr. Biol. 13 (2003) 230-235.

[9] P. T. Borges, C. V. Romao, L. M. Saraiva, V. L. Goncalves, M. A. Carrondo, M. Teixeira, C. Frazao, Analysis of a new flavodiiron core structural arrangement in Flv1-Delta FlR protein from Synechocystis sp. PCC6803, Journal of Structural Biology 205 (2019) 91-102.

[10] M. Ermakova, N. Battchikova, Y. Allahverdiyeva, E. M. Aro, Novel heterocyst-specific flavodiiron proteins in Anabaena sp PCC 7120, FEBS Letters 587 (2013) 82-87.

[11] P. Zhang, Y. Allahverdiyeva, M. Eisenhut, E. M. Aro, Flavodiiron proteins in oxygenic photosynthetic organisms: Photoprotection of photosystem II by Flv2 and Flv4 in *Synechocystis* sp PCC 6803, Plos One 4 (2009) 1-12.

[12] G. Shimakawa, K. Shaku, A. Nishi, R. Hayashi, H. Yamamoto, K. Sakamoto, A. Makino, C. Miyake, Flavodiiron2 and Flavodiiron4 Proteins Mediate An Oxygen-Dependent Alternative Electron Flow in Synechocystis Sp Pcc 6803 Under Co2-Limited Conditions, Plant Physiol. 167 (2015) 472-U732.

[13] A. Santana-Sanchez, D. Solymosi, H. Mustila, L. Bersanini, E. M. Aro, Y. Allahverdiyeva, Flavodiiron proteins 1-to-4 function in versatile combinations in O-2 photoreduction in cyanobacteria, Elife 8 (2019).

[14] H. Mustila, P. Paananen, N. Battchikova, A. Santana-Sanchez, D. Muth-Pawlak, M. Hagemann, E. M. Aro, Y. Allahverdiyeva, The Flavodiiron Protein Flv3 Functions as a Homo-Oligomer During Stress Acclimation and is Distinct from the Flv1/Flv3 Hetero-Oligomer Specific to the O-2 Photoreduction Pathway, Plant Cell Physiol. 57 (2016) 1468-1483.

[15] Y. Allahverdiyeva, H. Mustila, M. Ermakova, L. Bersanini, P. Richaud, G. Ajlani, N. Battchikova, L. Cournac, E. M. Aro, Flavodiiron proteins Flv1 and Flv3 enable cyanobacterial growth and photosynthesis under fluctuating light, Proc. Natl. Acad. Sci. U. S. A. 110 (2013) 4111-4116.

[16] F. Chaux, X. Johnson, P. Auroy, A. Beyly-Adriano, I. Te, S. Cuine, G. Peltier, PGRL1 and LHCSR3 Compensate for Each Other in Controlling Photosynthesis and Avoiding Photosystem I Photoinhibition during High Light Acclimation of Chlamydomonas Cells, Mol. Plant 10 (2017) 216-218.

[17] M. Ermakova, N. Battchikova, P. Richaud, H. Leino, S. Kosourov, J. Isojarvi, G. Peltier, E. Flores, L. Cournac, Y. Allahverdiyeva, E. M. Aro, Heterocyst-specific flavodiiron protein Flv3B enables oxic diazotrophic growth of the filamentous cyanobacterium Anabaena sp. PCC 7120, Proc. Natl. Acad. Sci. U. S. A. 111 (2014) 11205-11210.

[18] C. Gerotto, A. Alboresi, A. Meneghesso, M. Jokel, M. Suorsa, E. M. Aro, T. Morosinotto, Flavodiiron proteins act as safety valve for electrons in Physcomitrella patens, Proc. Natl. Acad. Sci. U. S. A. 113 (2016) 12322-12327.

[19] G. Shimakawa, K. Ishizaki, S. Tsukamoto, M. Tanaka, T. Sejima, C. Miyake, The Liverwort, Marchantia, Drives Alternative Electron Flow Using a Flavodiiron Protein to Protect PSI, Plant Physiol. 173 (2017) 1636-1647.

[20] G. Shimakawa, K. Shaku, C. Miyake, Oxidation of P700 in Photosystem I Is Essential for the Growth of Cyanobacteria, Plant Physiol. 172 (2016) 1443-1450.

[21] R. Gomez, N. Carrillo, M. P. Morelli, S. Tula, F. Shahinnia, M. R. Hajirezaei, A. F. Lodeyro, Faster photosynthetic induction in tobacco by expressing cyanobacterial flavodiiron proteins in chloroplasts, Photosynth. Res. (2017).

[22] S. Wada, H. Yamamoto, Y. Suzuki, W. Yamori, T. Shikanai, A. Makino, Flavodiiron Protein Substitutes for Cyclic Electron Flow without Competing CO2 Assimilation in Rice, Plant Physiol. 176 (2018) 1509-1518.

[23] H. Yamamoto, S. Takahashi, M. R. Badger, T. Shikanai, Artificial remodelling of alternative electron flow by flavodiiron proteins in Arabidopsis, Nature Plants 2 (2016).

[24] H. Yamamoto, T. Shikanai, PGR5-Dependent Cyclic Electron Flow Protects Photosystem I under Fluctuating Light at Donor and Acceptor Sides, Plant Physiol. 179 (2019) 588-600.

[25] K. A. Brown, Z. Guo, M. Tokmina-Lukaszewska, L. W. Scott, C. E. Lubner, S. Smolinski, D. W. Mulder, B. Bothner, P. W. King, The oxygen reduction reaction catalyzed by Synechocystis sp. PCC 6803 flavodiiron proteins, Sustainable Energy & Fuels 3 (2019) 3191-3200.

[26] M. Dann, D. Leister, Evidence that cyanobacterial Sll1217 functions analogously to PGRL1 in enhancing PGR5-dependent cyclic electron flow, Nature Communications 10 (2019).

[27] J. M. Schuller, J. A. Birrell, H. Tanaka, T. Konuma, H. Wulflhorst, N. Cox, S. K. Schuller, J. Thiemann, W. Lubitz, P. Sétif, T. Ikegami, B. D. Engel, G. Kurisu, M. M. Nowaczyk, Structural adaptations of photosynthetic complex I enable ferredoxin-dependent electron transfer, Science 363 (2019) 257-260.

[28] H. Yamamoto, T. Shikanai, In Planta Mutagenesis of Src Homology 3 Domain-like Fold of NdhS, a Ferredoxin-binding Subunit of the Chloroplast NADH Dehydrogenase-like Complex in Arabidopsis A CONSERVED ARG-193 PLAYS A CRITICAL ROLE IN FERREDOXIN BINDING, J. Biol. Chem. 288 (2013) 36328-36337.

[29] F. Gao, J. Zhao, L. Chen, N. Battchikova, Z. Ran, E. M. Aro, T. Ogawa, W. Ma, The NDH-1L-PSI Supercomplex Is Important for Efficient Cyclic Electron Transport in Cyanobacteria, Plant Physiol. 172 (2016) 1451-1464.

[30] X. Qin, X. Pi, W. Wang, G. Han, L. Zhu, M. Liu, L. Cheng, J. R. Shen, T. Kuang, S. F. Sui, Structure of a green algal photosystem I in complex with a large number of light-harvesting complex I subunits, Nature Plants 5 (2019) 263-272.

[31] Y. Mazor, A. Borovikova, N. Nelson, The structure of plant photosystem I super-complex at 2.8 angstrom resolution, Elife 4 (2015).

[32] P. Jordan, P. Fromme, H. T. Witt, O. Klukas, W. Saenger, N. Krauss, Three-dimensional structure of cyanobacterial photosystem I at 2.5 Å resolution, Nature 411 (2001) 909-917.

[33] C. Klughammer, U. Schreiber, Deconvolution of ferredoxin, plastocyanin, and P700 transmittance changes in intact leaves with a new type of kinetic LED array spectrophotometer, Photosynth. Res. 128 (2016) 195-214.

[34] U. Schreiber, C. Klughammer, Analysis of photosystem I donor and acceptor sides with a new type of online-deconvoluting kinetic LED-array spectrophotometer, Plant Cell Physiol. 57 (2016) 1454-1467.

[35] U. Schreiber, Redox changes of ferredoxin, P700, and plastocyanin measured simultaneously in intact leaves, Photosynth. Res. 134 (2017) 343-360.

[36] H. Ohkawa, H. B. Pakrasi, T. Ogawa, Two types of functionally distinct NAD(P)H dehydrogenases in Synechocystis sp strain PCC6803, J. Biol. Chem. 275 (2000) 31630-31634.

[37] J. G. K. Williams, Construction of Specific Mutations in Photosystem-Ii Photosynthetic Reaction Center by Genetic-Engineering Methods in Synechocystis-6803, Methods in Enzymology 167 (1988) 766-778.

[38] G. Shimakawa, P. Sétif, A. Krieger-Liszkay, Near infrared in vivo measurements of photosystem I and its lumenal electron donors with a recently-developed spectrophotometer, Photosynth. Res. 144 (2020) 63-72.

[39] J. Kauny, P. Sétif, NADPH fluorescence in the cyanobacterium *Synechocystis* sp. PCC 6803: A versatile probe for *in vivo* measurements of rates, yields and pools, Biochim. Biophys. Acta 1837 (2014) 792-801.

[40] G. Schreiber, C. Klughammer, New NADPH/9-AA module for the DUAL-PAM-100: Description, operation and examples of application, PAM Applic. Notes 2 (2009) 1-13.

[41] P. Sétif, A. Boussac, A. Krieger-Liszkay, Near-infrared in vitro measurements of photosystem I cofactors and electron-transfer partners with a recently developed spectrophotometer, Photosynth. Res. 142 (2019) 307-319.

[42] P. Sétif, Electron-transfer kinetics in cyanobacterial cells: Methyl viologen is a poor inhibitor of linear electron flow, Biochim. Biophys. Acta 1847 (2015) 212-222.

[43] A. A. Bulychev, A. A. Cherkashin, E. M. Muronets, I. V. Elanskaya, Photoinduction of electron transport on the acceptor side of PSI in Synechocystis PCC 6803 mutant deficient in flavodiiron proteins Flv1 and Flv3, Biochim. Biophys. Acta 1859 (2018) 1086-1095.

[44] P. Ilik, A. Pavlovic, R. Kouril, A. Alboresi, T. Morosinotto, Y. Allahverdiyeva, E. M. Aro, H. Yamamoto, T. Shikanai, Alternative electron transport mediated by flavodiiron proteins is operational in organisms from cyanobacteria up to gymnosperms, New Phytol. (2017).

[45] G. Shimakawa, C. Miyake, Oxidation of P700 Ensures Robust Photosynthesis, Frontiers in Plant Science 9 (2018).

[46] G. Moal, B. Lagoutte, Photo-induced electron transfer from photosystem I to $NADP^+$: Characterization and tentative simulation of the *in vivo* environment, Biochim. Biophys. Acta 1817 (2012) 1635-1645.

[47] N. Yeremenko, R. Jeanjean, P. Prommeenate, V. Krasikov, P. J. Nixon, W. F. J. Vermaas, M. Havaux, H. C. P. Matthijs, Open reading frame ssr2016 is required for antimycin A-sensitive photosystem I-driven cyclic electron flow in the cyanobacterium *Synechocystis* sp PCC 6803, Plant Cell Physiol. 46 (2005) 1433-1436.

[48] N. Battchikova, E. M. Aro, Cyanobacterial NDH-1 complexes: multiplicity in function and subunit composition, Physiol. Plant. 131 (2007) 22-32.

[49] G. T. Hanke, Y. Satomi, K. Shinmura, T. Takao, T. Hase, A screen for potential ferredoxin electron transfer partners uncovers new, redox dependent interactions, Biochim. Biophys. Acta 1814 (2011) 366-374.

[50] E. A. Peden, M. Boehm, D. W. Mulder, R. Davis, W. M. Old, P. W. King, M. L. Ghirardi, A. Dubini, Identification of Global Ferredoxin Interaction Networks in Chlamydomonas reinhardtii, J. Biol. Chem. 288 (2013) 35192-35209.

[51] L. Nikkanen, A. Santana-Sanchez, M. Ermakova, M. Rögner, L. Cournac, Y. Allahverdiyeva, Functional redundancy between flavodiiron proteins and NDH-1 in *Synechocystis* sp. PCC 6803, Plant J. in press (2020).

[52] F. Chaux, A. Burlacot, M. Mekhalfi, P. Auroy, S. Blangy, P. Richaud, G. Peltier, Flavodiiron proteins promote fast and transient O2 photoreduction in Chlamydomonas, Plant Physiol. (2017).

[53] N. Battchikova, L. Z. Wei, L. Y. Du, L. Bersanini, E. M. Aro, W. M. Ma, Identification of novel Ssl0352 protein (NdhS), essential for efficient operation of cyclic electron transport around photosystem I, in NADPH:plastoquinone oxidoreductase (NDH-1) complexes of *Synechocystis* sp. PCC 6803, J. Biol. Chem. 286 (2011) 36992-37001.

[54] X. Wang, F. Gao, J. Zhang, J. Zhao, T. Ogawa, W. Ma, A Cytoplasmic Protein Ssl3829 Is Important for NDH-1 Hydrophilic Arm Assembly in Synechocystis sp. Strain PCC 6803, Plant Physiol. 171 (2016) 864-877.

[55] J. Zhang, F. Gao, J. Zhao, T. Ogawa, Q. Wang, W. Ma, NdhP Is an Exclusive Subunit of Large Complex of NADPH Dehydrogenase Essential to Stabilize the Complex in Synechocystis sp Strain PCC 6803, J. Biol. Chem. 289 (2014) 18770-18781.

[56] J. Zhao, W. Rong, F. Gao, T. Ogawa, W. Ma, Subunit Q Is Required to Stabilize the Large Complex of NADPH Dehydrogenase in Synechocystis sp. Strain PCC 6803, Plant Physiol. 168 (2015) 443-451.

[57] C. Klughammer, U. Schreiber, Saturation Pulse method for assessment of energy conversion in PS I, PAM Applic. Notes 1 (2008) 11-14.

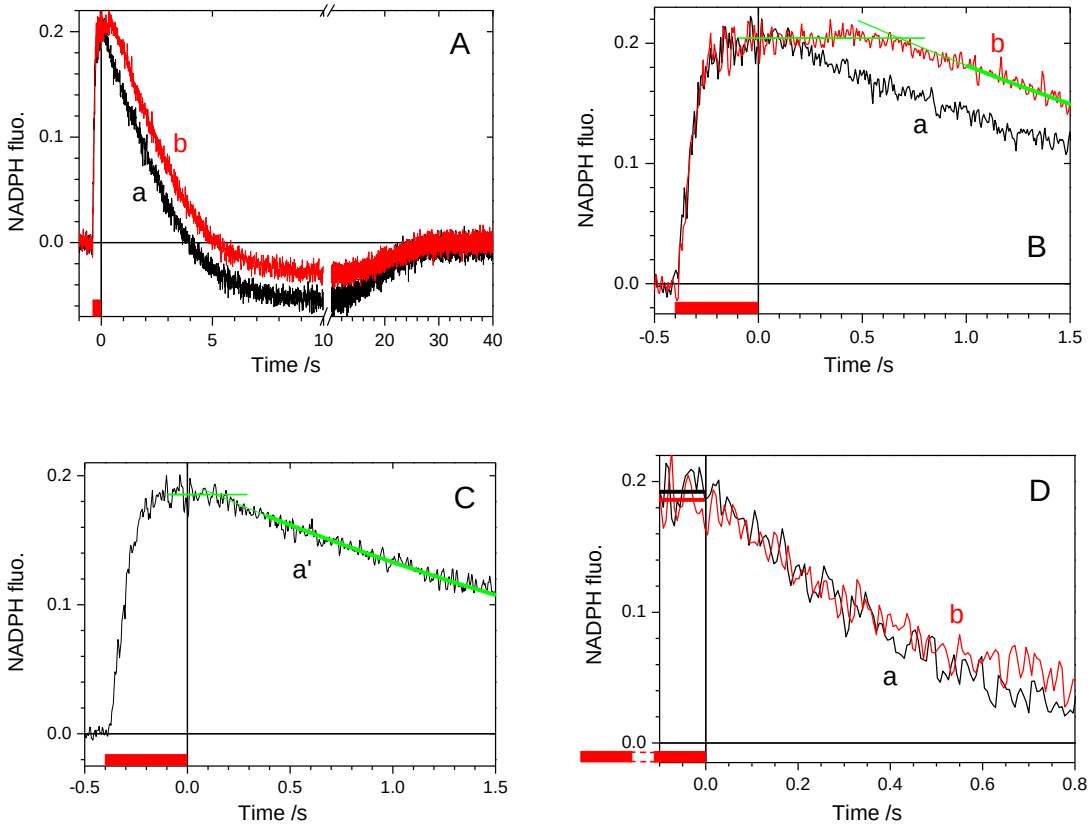

Fig. 1. NADPH fluorescence kinetics in WT and Δ*flv1/3* cells.

Cells were studied at a concentration of 4 µg Chl./ml. The dark fluorescence levels were set at 0 and time was set at 0 at the end of illumination. Illumination time is indicated by a red bar at the bottom of all parts. **A** and **B**. The same signals induced by a 400 ms illumination period are shown on 2 different time scales. Δ*flv1/3* signals (red, traces b) were multiplied by a factor of 1.04 for easier comparison of the kinetics with those of WT (black, traces a). In B, the continuous green line corresponds to a monoexponential fit of Δ*flv1/3* signal (thick line) which was extended to shorter times (thin line). This line crosses the fluorescence level at the end of illumination (horizontal green line) at *c*. 700 ms after the end of illumination. Actinic light intensity of 700 µmoles photons $m^{-2}s^{-1}$. **C**. A similar experiment was performed with extensive averaging with WT cells. The same procedure as in B was used to get a crossing point at 140 ms. Averages of 25 (A and B) or 80 measurements (C) separated by 1 min. time intervals. **D**. the same cells as in A and B were later on illuminated for 120 s at an intensity of 350 µmoles photons $m^{-2}s^{-1}$. The signal levels at the end of illumination (fitted with a constant amplitude between -5 s and 0) are shown as horizontal lines. Averages of 5 measurements separated by 6 min. time intervals. Cells were initially dark-adapted for 8 min.

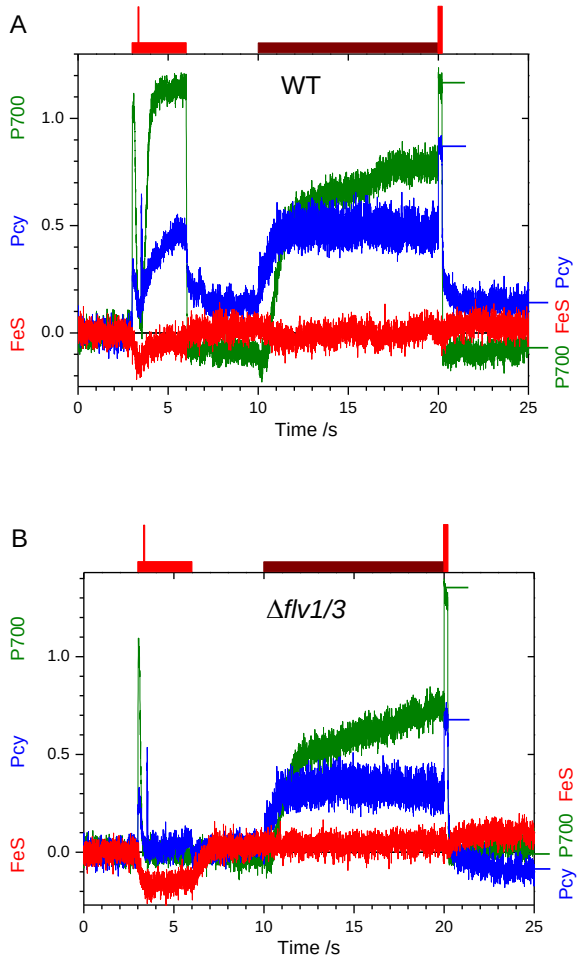

Fig. 2. Maximum amplitudes of P700, Pcy and iron-sulfur signals in WT and Δ*flv1/3* cells determined by NIR absorption.

Signals (P700, green; Pcy, blue; FeS, red) were measured in WT (part A, 12.5 µg Chl./ml) and Δ*flv1/3* (part B, 12.8 µg Chl./ml) cells under red actinic light (from 3 to 6 s, 930 µmoles photons $m^{-2}s^{-1}$) and just after far red light (from 10 to 20 s) by using MT pulses (25,000 µmoles photons $m^{-2}s^{-1}$) of 30 ms duration (under red light, MT begins at 3.35 s) or 200 ms duration (MT begins when far red light is switched off). Horizontal marks indicate the maximum intensity levels under light or the zero levels at the end of illumination (P700 and Pcy). The calculated signals are given in Table 2. Cells were initially dark-adapted for 8 min. One single measurement in each case. Vertical scales are in ($\Delta I/I \times 10^{-3}$) at 902.5 nm. The illumination protocol is indicated at the top of the figures (red and dark red colors for red and far red light, respectively).

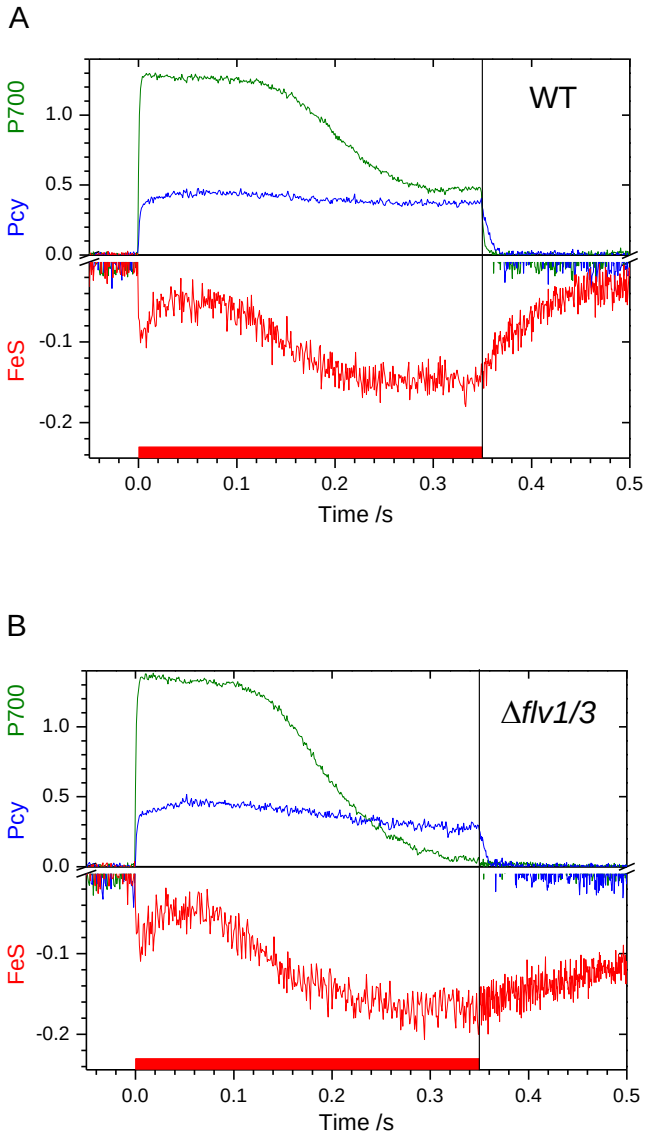

Fig. 3. P700, Pcy and FeS signals in WT and Δ*flv1/3* cells under and after a short illumination.

The same cell suspensions used in Fig. 2 were submitted to high intensity red illumination (8,100 µmoles photons $m^{-2}s^{-1}$) for 350 ms, a time at which a minimum is observed in the WT $P700^{+}$ signal. Note that the Y-scales are different for the upper and lower parts of each figure. Averages of 20 measurements, separated by 1 min. time intervals. Cells were initially dark-adapted for 8 min. The red rectangles at the bottom of the kinetics indicate the periods of illumination. Vertical scales are given in ($\Delta I/I \times 10^{-3}$) at 902.5 nm.

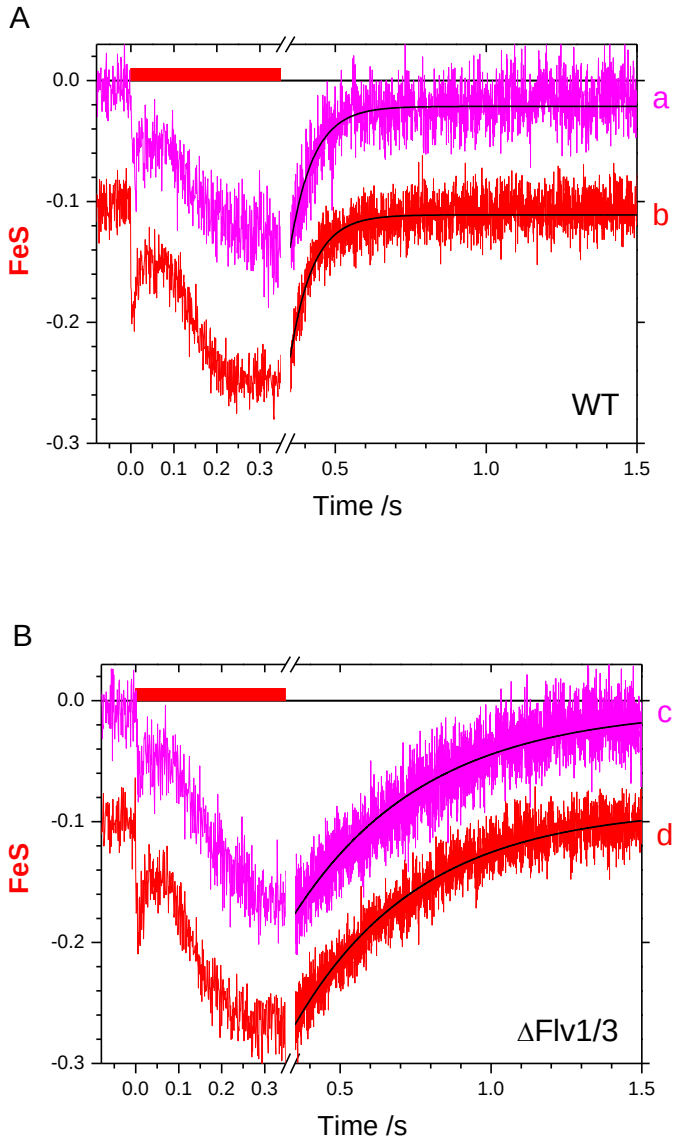

Fig. 4. FeS signals in WT and Δ*flv1/3* cells under and after a short illumination.

Red traces are those of Fig 3 (shifted by -0.1) and magenta ones were obtained with the same samples under similar conditions but at lower light intensity (1,170 µmoles photons $m^{-2}s^{-1}$). Note a break in the X-scale. All decay kinetics were fitted (black traces) with single exponentials (A × exp[-k(t-0.35)] + B), resulting in rates of 13.1, 13.3, 2.3 and 2.4 s^{-1} for traces a, b, c and d, respectively. The red rectangles above the baseline indicate the periods of illumination. Cells were initially dark-adapted for 8 min. Vertical scales are given in ($\Delta I/I \times 10^{-3}$) at 902.5 nm.

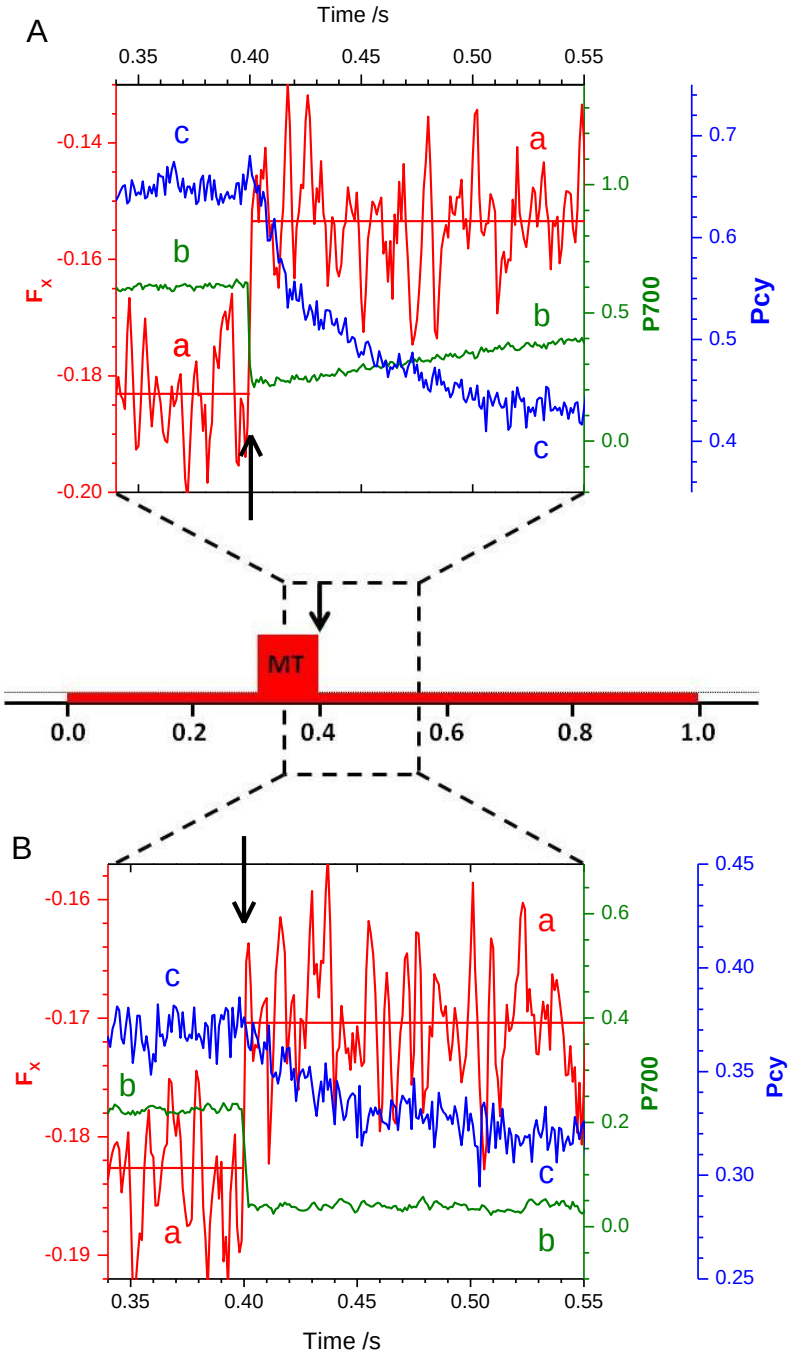

Fig. 5. Evidence for recombination between $P700^+$ and F_{Xred}

WT (A) and Δ*flv1/3* (B) cells at concentrations identical to those of Figures 3 and 4 were submitted from 0 to 1 s to red actinic light (2,200 µmoles photons $m^{-2}s^{-1}$) and between 0.3 and 0.4 s to a 100 ms MT pulse (40,000 µmoles photons $m^{-2}s^{-1}$). Kinetics of P700 (trace b, green), Pcy (trace c, blue) and FeS/F_X (trace a, red) are shown at the end of the MT pulse, which is indicated by a vertical arrow. The middle part of the figure shows the illumination sequence with the dashed rectangle showing the region which is zoomed in the upper and lower part. The Y-scales of the 3 species are shown with different colors in ($\Delta I/I \times 10^{-3}$) at 902.5 nm with all signals set to 0 before illumination. For part B, the Y-scales are expanded twice relative to part A. In each part, the full vertical scales of the different species (P700, Pcy and F_X) are proportional to their relative absorption coefficients (Table 1: 1, 0.252 and -0.044 for P700, Pcy and (F_A F_B), respectively), so that the signal amplitudes can be directly compared. Thus recombination between $P700^+$ and F_{Xred} should give similar apparent

amplitudes, if F_X reduction gives a signal identical to that of single (F_A F_B) reduction. Cells were initially dark-adapted for 8 min. Averages of 40 measurements, separated by 1 min. time intervals.

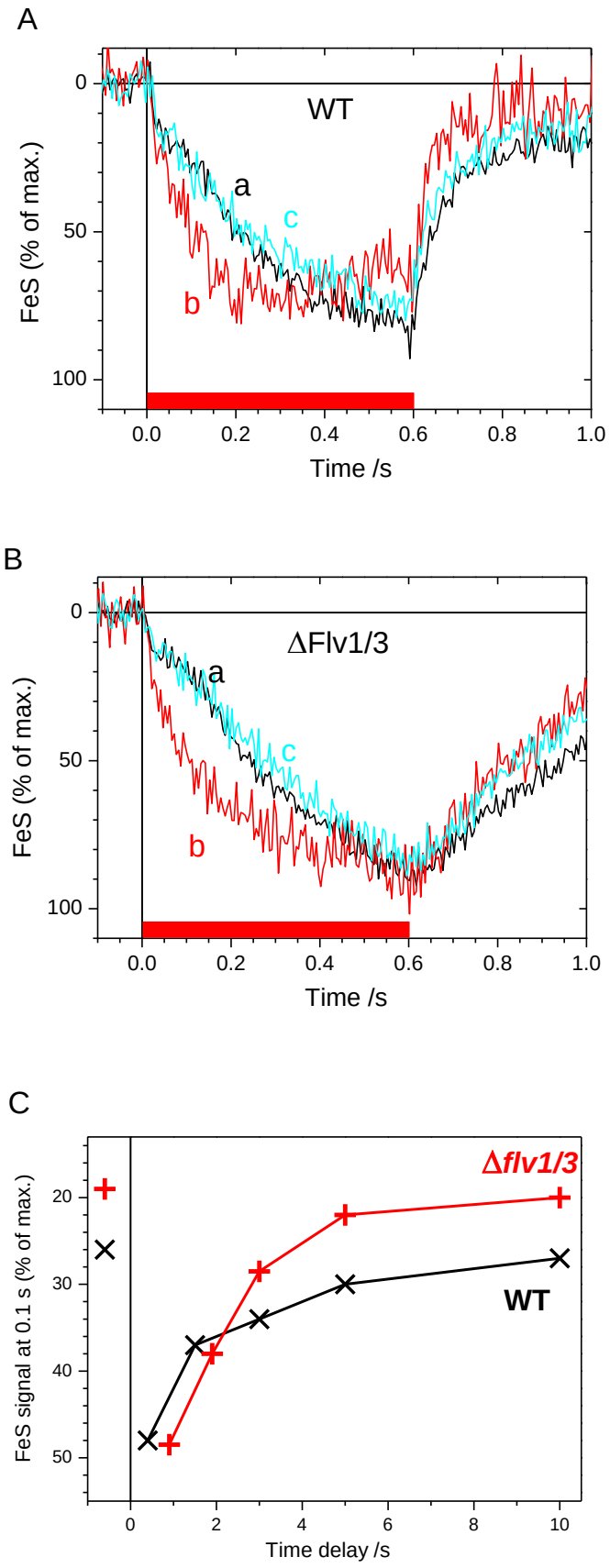

Fig. 6. Dependence of the kinetics of FeS reduction on the NADPH level.

FeS reduction was measured during two consecutive periods of 0.6 s red light illumination (hν) periods at an intensity of 250 μmoles photons $m^{-2}s^{-1}$. **A**. WT, a (black), first hν; b (red), second hν starting 0.4 s after the end of the 1st hν; c (cyan), average of signals with the second hν starting 5 and 10 s after the end of the 1st hν. **B**. Δ*flv1/3*, similar signals as in A, except that trace b was measured with a delay of 0.9 s, which is necessary for the almost complete reoxidation of FeS. **C**. The FeS signal, which was measured at 0.1 s after the beginning of the 2nd hν, is plotted as a function of the delay time between the end of the 1st hν and the beginning of the 2nd hν. The 1st hν signal at 0.1 s is shown on the upper left of the figure (t < 0). WT (black crosses, x) and Δ*flv1/3* (red plus signs, +). Both strains were at *c*. 9 μg chl./ml. Signals are plotted as a function of the maximum FeS signal intensities that were recorded as in Fig. 2. Traces a, b and c are averages of 100, 20 and 40 measurements, respectively. Measurements are separated by 1 min. time intervals. The red rectangles at the bottom of the kinetics (A/B) indicate the periods of illumination. Cells were initially dark-adapted for 8 min. Vertical scales in ($\Delta I/I \times 10^3$) at 902.5 nm.

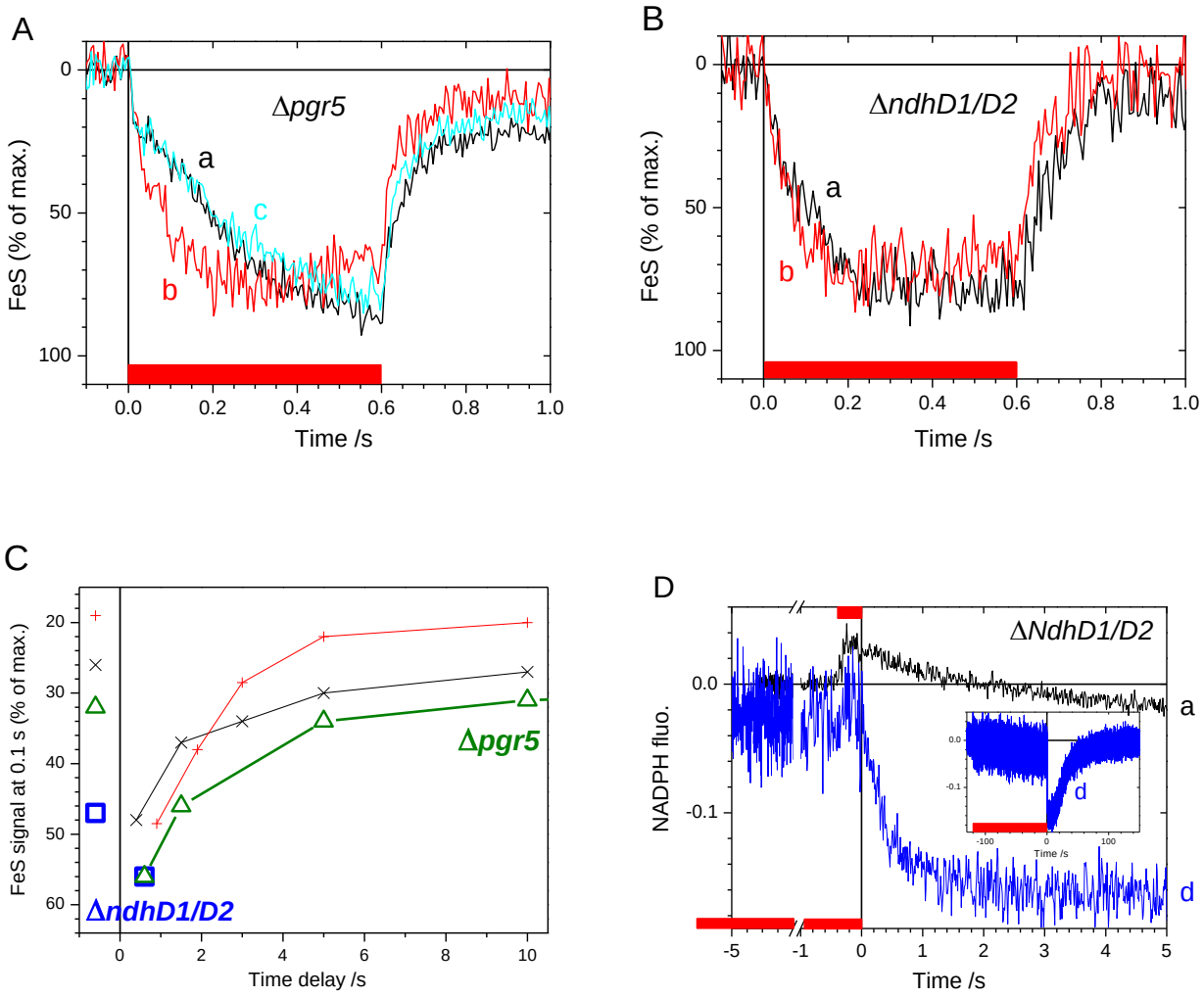

Fig. 7. Kinetics properties of Δ*pgr5* and Δ*ndhD1/D2* cells.

Parts **A** and **B**: Experimental conditions are identical to those of Fig. 6. FeS reduction was measured during two consecutive periods of 0.6 s red light illumination (hν) periods at an intensity of 250 µmoles photons $m^{-2}s^{-1}$. Trace a: 1st hν. Trace b: 2nd hν beginning 0.6 s after end of 1st. Trace c (for Δ*pgr5*): 2nd hν beginning 5, 10 and 20 s (signal average) after end of 1st hν. Δ*pgr5*: averages of 90, 20 and 50 measurements for traces a, b and c, respectively. Δ*ndhD1/D2*: averages of 10 measurements for both traces. Individual measurements are separated by 1 min. time intervals. The red rectangles indicate the period of illumination. Cells were initially dark-adapted for 8 min. Signals are shown in percent of the maximum FeS_{red} signal amplitude.**C**. The FeS signal, which was measured at 0.1 s after the beginning of the 2nd hν, is plotted as a function of the delay time between the end of the 1st hν and the beginning of the 2nd hν. The 1st hν signal at 0.1 s is shown on the upper left of the figure (t < 0). Δ*pgr5* (green triangles) and Δ*ndhD1/D2* (blue squares). Data of Fig. 6C are also shown with thin lines and small symbols for the sake of comparison (black x for WT and red + for Δ*flv1/3*). **D**. NADPH fluorescence kinetics in Δ*ndhD1/D2* cells. Trace a (black): red actinic light illumination of 400 ms was given to a dark-adapted sample (700 µmoles photons $m^{-2}s^{-1}$, average of 30 measurements separated by 1 min. time intervals). Trace d (blue): the sample was later on submitted to a prolonged red light illumination of 120 s (350 µmoles photons $m^{-2}s^{-1}$, average of 5 measurements separated by 6 mins. time intervals). For both traces, the fluorescence levels in the dark before illumination were set at 0 and time 0 corresponds to the end of illumination. The inset shows the fluorescence kinetics corresponding to trace d on a longer time scale. The red rectangles at the bottom of the kinetics (and at the top for trace a) indicate the periods of illumination. Chl. concentration (D) was *c*. 4 µg/ml.

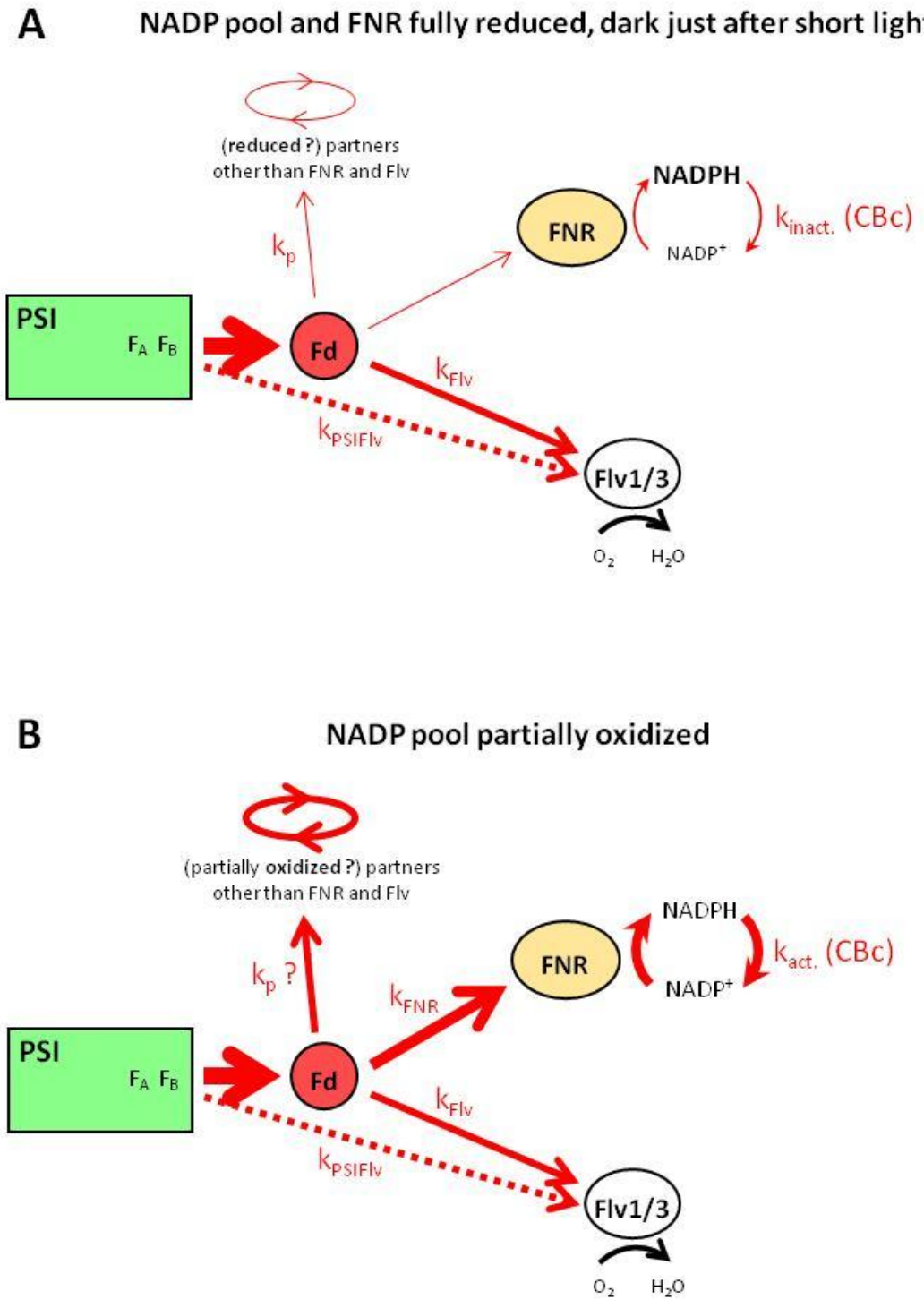

Fig. 8. Electron transfer scheme involving the acceptor side of PSI.

Part **A** corresponds to the situation encountered in Figures (1, 3-4), where FNR and the NADP pool are fully reduced and with a poorly activated or inactivated CBc. Fd_{red} has many partners other than FNR or Flv1/3 (NDH1-L, enzymes involved in nitrogen assimilation, etc...) giving a global rate k_p of Fd_{red} oxidation. From the present KLAS-NIR measurements: $k_{Flv} = 11\ s^{-1}$; $k_p + k_{inact.} = 2.3\ s^{-1}$. $k_{inact.}$ is defined as a Fd_{red} oxidation rate corresponding to the slow rate of NADPH oxidation which limits the

electron transfer pathway: Fd → FNR → NADPH → substrates . The relative values of k_p and $k_{inact.}$ cannot be deduced from the present work. The dotted arrow from F_B to Flv indicates that direct reduction of Flv by PSI cannot be excluded from our data. Part **B** corresponds to situations where the NADP pool is not completely reduced because of CBc activation (rate $k_{act.}$) and where the rate k_p is hypothetically assumed to be larger than in A (see text). From the kinetics of NADPH photoreduction: $k_{FNR} \geq 100\ s^{-1}$.

Supplementary Figures

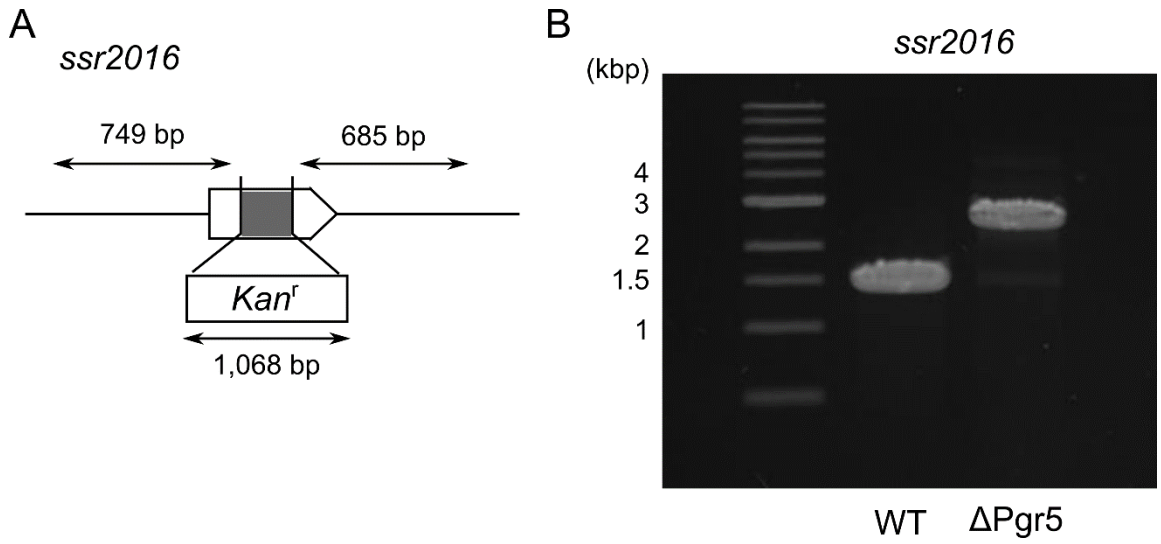

Fig. SI1. Insertional inactivation of the *pgr5* gene in *Syn. 6803*.

(A) Physical map of the insertion site of antibiotic resistance cassette in Δ*pgr5*. The arrowheads indicate the locations of PCR primers. The lengths of the amplified DNA fragments are shown. The full length of the gene is 198 bp. The shaded box indicates the removed genome DNA region (33 bp). (B) DNA fragments amplified by PCR showing complete segregation of the inactivated gene.

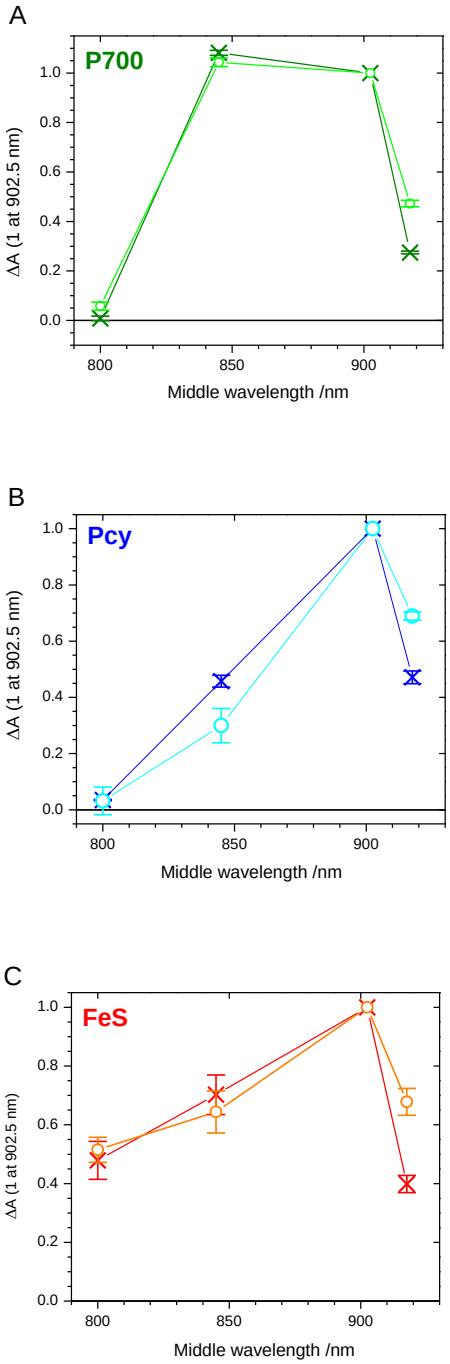

Fig. SI2. Differential model plots of P700 (**A**), Pcy (**B**) and FeS (**C**).

All spectra are normalized to 1 at the middle wavelength of 902.5 nm. The spectra shown as crosses were used in the present study and were measured in Kobe university with the *Syn*. 6803 WT and Δ*flv1/3* strains from Kobe (averages of 3 measurements). The spectra shown as open circles were measured in the Saclay laboratory with the same WT strain (averages of 2 measurements). All measurements were performed at 25°C.

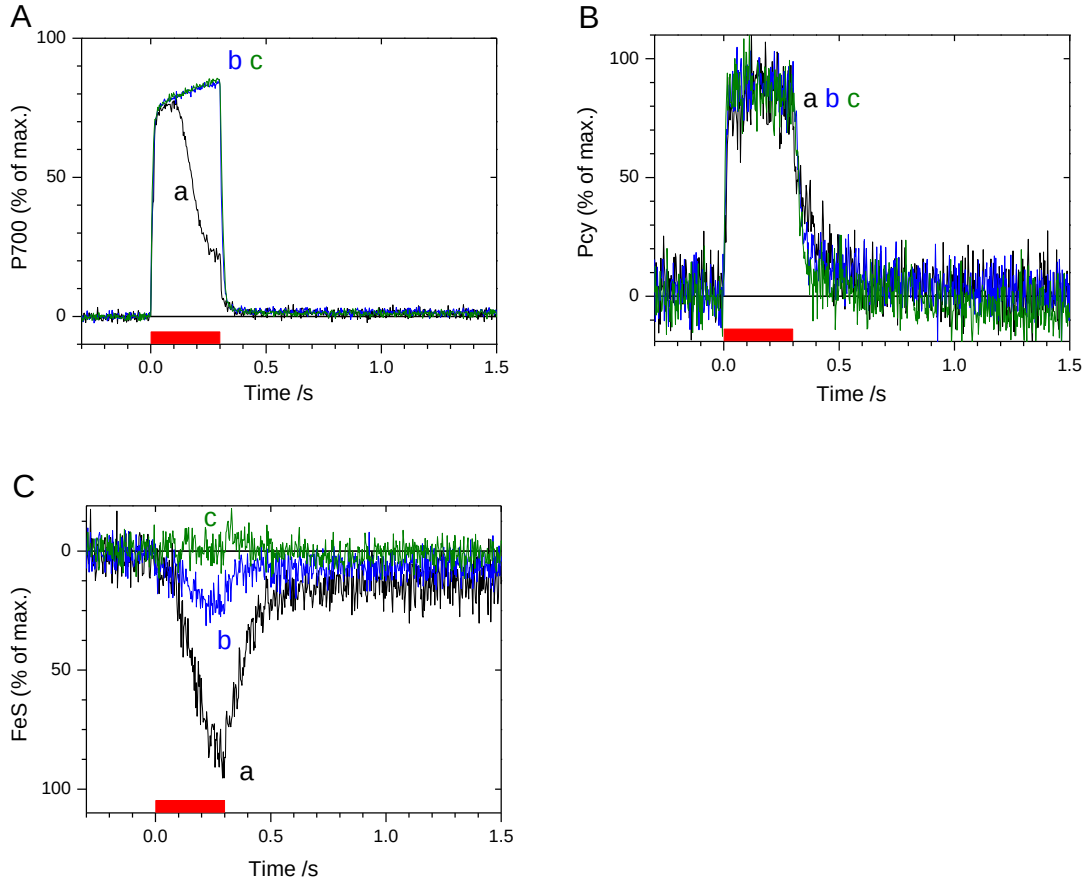

Fig. SI3. Effect of methyl viologen (MV) on P700 (**A**), Pcy (**B**) and FeS (**C**) signals.

300 ms pulses of high intensity (14,500 µmoles photons $m^{-2}s^{-1}$) were given to a concentrated suspension of WT cells (*c*. 45 µg chl. ml). Traces a were recorded before MV addition. Then 3 measurements were averaged between 7 and 9 min. (traces b) and between 18 and 20 min. (traces c) after addition of 300 µM MV. Measurements are separated by 1 min. time intervals.

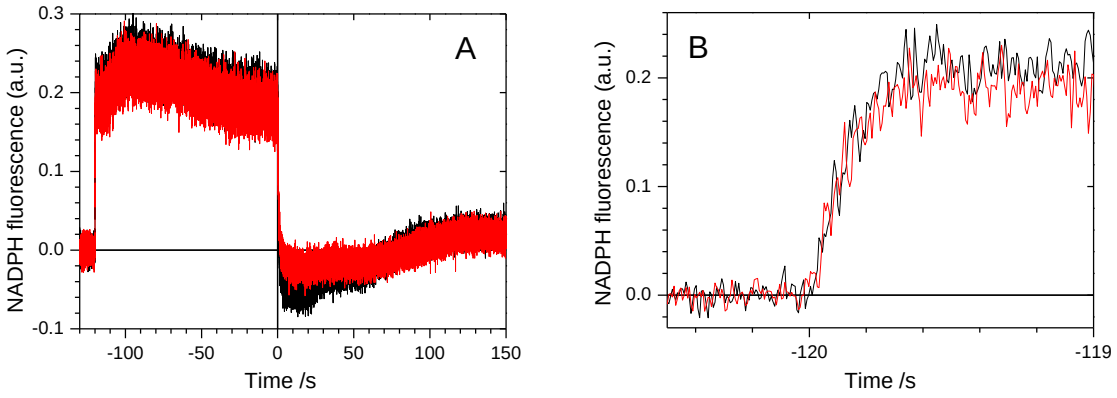

Fig. SI4. NADPH fluorescence kinetics with a 120 s illumination period.

The same cell suspensions of WT (black traces) and Δ*flv1/3* (red traces) as those of Fig. 1 were later on illuminated for 120 s at a light intensity of 350 µmoles photons $m^{-2}s^{-1}$. The dark fluorescence levels before illumination were set at 0 and time origin was set at the end of illumination. **B** is a zoomed view of **A** at the onset of illumination. The decay kinetics at the end of illumination are shown in Fig. 1D.

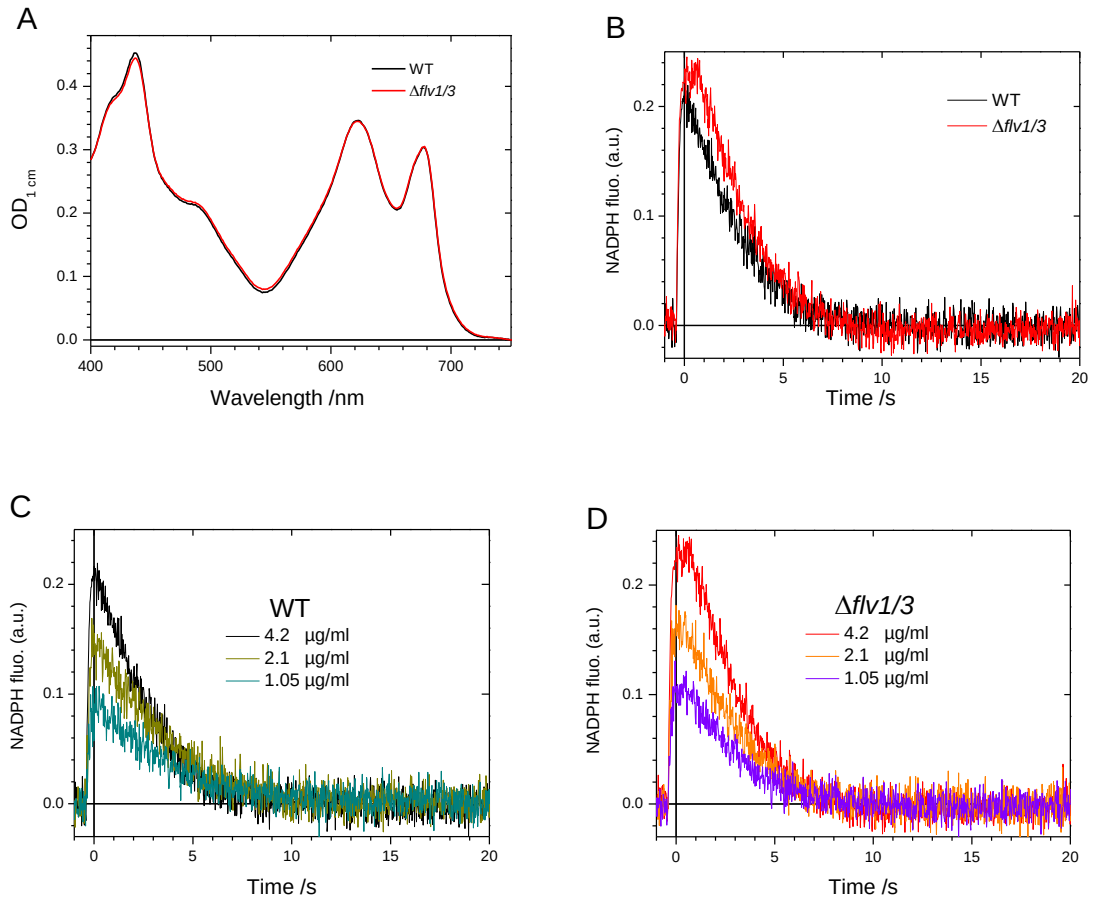

Fig. SI5. NADPH fluorescence kinetics at different chlorophyll concentrations.
Cell suspensions of WT and Δ*flv1/3* were adjusted at the same chlorophyll concentration of 4.2 µg/mL by measuring their absorption spectra (A; Shimakawa et al., 2020) before recording light-induced NADPH fluorescence signals (B). Cells were then diluted 2 and 4 times before repeating the measurements (C and D). Signal sizes decrease with chlorophyll content, although less than linearly, as previously reported in this range of chlorophyll concentrations (Kauny and Sétif, 2014). Measurements conditions are similar to those of Fig. 1A, except only 10 measurements were averaged with time intervals of 3 mins. between consecutive measurements. With this time interval, no signal undershoot was observed contrary to Fig. 1A (1 min. time intervals). The Δ*flv1/3* to WT ratio of signals is 1.10.

J. Kauny, P. Sétif (2014) Biochim. Biophys. Acta 1837:792-801.
G. Shimakawa, P. Sétif, A. Krieger-Liszkay (2020) Photosynth. Res. 144:63-72.

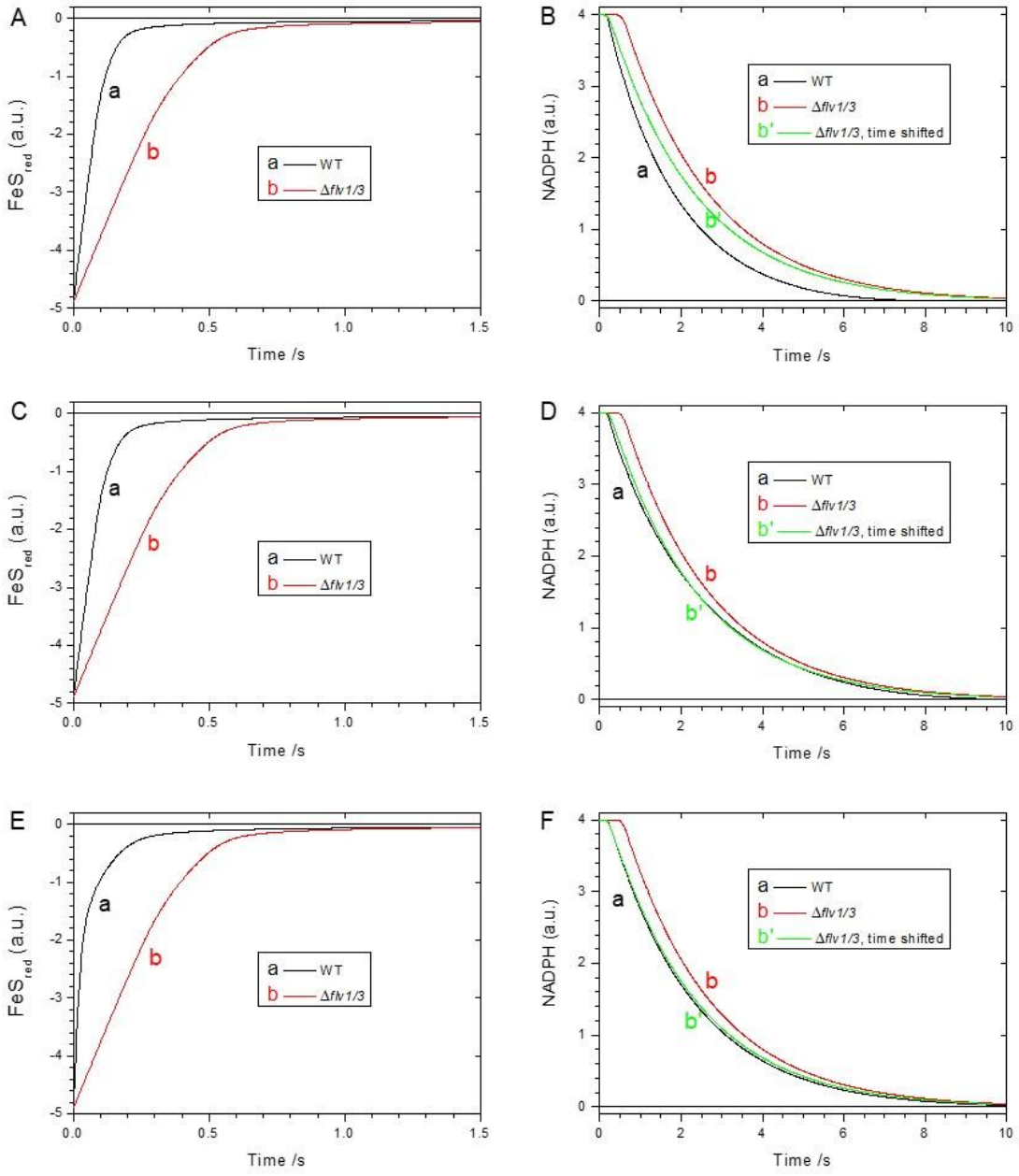

Fig. SI6. Simulations of FeS_{red} and NADPH decay kinetics.
These simulations (Mathematica 6.0, Wolfram Research, Inc., Champaign, IL, 2007) were done to qualitatively reproduce salient features of the kinetic differences between WT and Δ*flv1/3* strains following a short illumination (Figures 1 and 4), but it was not attempted to quantitatively reproduce these kinetics.
FeS_{red} (left, A/C/E) and NADPH (right, B/D/F) decay kinetics in darkness following illumination were simulated (arbitrary units) for three different sets of kinetic rate constants (A/B, C/D and E/F). Traces a (black) and b (red) were calculated for WT and Δ*flv1/3*, respectively. Traces b' (Δ*flv1/3*) of NADPH decay (green) are identical to traces b, except for a time shift of -0.34 s. This shift was chosen so that the initial NADPH decay of traces a and b' occur simultaneously.

<u>Conditions and parameters common to all cases:</u> a) the Fd to PSI ratio is 1.5. **b)** Fd and (F_A F_B) are 100% reduced at t = 0. **c)** Double reduction of (F_A F_B) leads to a signal = 2 × 1.7 = 3.4 times larger than reduction of 1 Fd (Table 1). **d)** The redox equilibria between (F_A F_B), Fd and NADPH are very fast *vs*

oxidizing reactions*, i.e.* these 3 species are at any time in pre-equilibrium conditions. The equilibrium constants K_1, K_2 and K_3, for the 3 following reactions:

(1) $(F_A\ F_B)_{1red} + Fd_{ox} \Leftrightarrow (F_A\ F_B)_{ox} + Fd_{red}$
(2) $(F_A\ F_B)_{2red} + Fd_{ox} \Leftrightarrow (F_A\ F_B)_{1red} + Fd_{red}$
(3) $2\ Fd_{red} + NADP^+ + H^+ \Leftrightarrow 2\ Fd_{ox} + NADPH$

are taken to be 30, 100 and 1100, respectively. This corresponds to the following differences of midpoint potentials:

$E_m((F_A\ F_B)_{ox}/(F_A\ F_B)_{1red}) - E_m(Fd_{ox}/Fd_{red}) = -87$ mV

$E_m((F_A\ F_B)_{1red}/(F_A\ F_B)_{2red}) - E_m(Fd_{ox}/Fd_{red}) = -118$ mV

$E_m(Fd_{ox}/Fd_{red}) - E_m(NADP^+/NADPH) = -90$ mV. In this case, the $NADP^+$/NADPH equilibrium involves a 2-electrons reaction, hence the large value of K_3.

e) The NADP pool to PSI ratio is 4.0 and NADP is 100% reduced at t = 0. This pool size corresponds to the upper limit of the NADP photoreducible pool size that was previously determined in *Syn*. 6803 (Kauny and Sétif, 2014). **f)** The total rate k_p of Fd_{red} oxidation by partners other than FNR and Flv has a value of 2 s^{-1} (see Fig. 8)

<u>Parameters specific to different cases</u> (see Fig. 8 for the definition of rate constants):

Parts A and B: Flv is reduced by Fd. k_{Flv} = 11 s^{-1} and 0 for WT and Δ*flv1/3*, respectively; k_{PSIFlv} = 0 for both strains; k_{CBC} = 0.45 s^{-1} for both strains. k_{CBC} is the rate of NADPH consumption resulting from a non or poorly activated CBc (k_{inact} in Fig. 8). It also incorporates all other processes that directly oxidize NADPH. As discussed in the main text, the lags in NADPH decay kinetics (B) are associated to the presence of FeS_{red} (A), which maintains the NADP pool to its fully reduced state. Comparison of traces a and b' of NADPH decay kinetics (B) shows that, disregarding the different lags, the NADPH decay is slightly slower in Δ*flv1/3*. This small difference in simulation decays results from energetically uphill reduction of Fd by NADPH followed by Fd_{red} oxidation by Flv in WT.

Parts C and D: same rates as in A/B, except that k_{CBC} = 0.3 and 0.45 s^{-1} for WT and Δ*flv1/3*, respectively. The change in k_{CBC} rate for WT results in no visible change in the FeS_{red} decay kinetics (C). However, traces a and b' of NADPH decay (D) exhibit similar decay kinetics, contrary to B but similarly to our experimental observations (Fig. 1/A and Fig. SI5). This suggests that some slow NADPH-consuming processes are a little faster in Δ*flv1/3 vs* WT and this effect compensates the effect of energetically uphill reduction of Fd by NADPH which occurs in WT (B)

Parts E and F: Flv is reduced by $(F_A\ F_B)_{red}$. k_{Flv} = 0 for both strains and k_{PSIFlv} = 60 s^{-1} and 0 for WT and Δ*flv1/3*, respectively; k_{CBC} = 0.45 s^{-1} for both strains. Traces a and b' (F) exhibit similar decay kinetics, which is attributed to the fact that reduction of $(F_A\ F_B)$ by NADPH (relayed by Fd) is too energetically uphill to have an effect on NADPH decay kinetics in WT. The FeS_{red} decay kinetics in WT exhibit, as expected, a biphasic character (trace a). This character was not identified in our WT measurements, but cannot be completely excluded in view of the poor signal-to-noise ratio of the FeS_{red} signals and the possible kinetic distortions due to imperfect KLAS-NIR signal deconcolutions, as discussed in the main text.

J. Kauny, P. Sétif (2014) Biochim. Biophys. Acta 1837:792-801.